NOTE TO USERS

Power Transients in Fiber Raman Amplifiers with Coherent Pumping or Incoherent Pumping

Guoshun Zhan

A Thesis

In

The Department of Electrical and Computer Engineering

Presented in Partial Fulfillment of the Requirements

for the Degree of Master of Applied Science at

Concordia University

Montreal, Quebec, Canada

Your file Votre référence
ISBN: 0-494-10259-4
Our file Notre référence
ISBN: 0-494-10259-4

Abstract

Power Transients in Fiber Raman Amplifiers

with Coherent Pumping or Incoherent Pumping

Guoshun Zhan

We investigate power transient effect caused by channel addition/removal in fiber Raman amplifiers (FRAs). A comprehensive large-signal numerical model of FRAs, which incorporates time variation effects, and downstream and upstream propagations of multiple signals, pumps, and amplified spontaneous emission components, is developed and used for the theoretical analysis. The effect of pumping schemes, input signal power, pump power, the length and type of Raman fiber, and the number of added or dropped channels on the dynamics of surviving channel power fluctuations is studied. Three different drop/add cases are considered: (a) L band drop/add, (b) C band drop/add, (c) every other channel drop/add. For all three cases, power transient behaviors in fiber Raman amplifiers counter-pumped by multiple coherent pumps or multiple incoherent pumps are analyzed at the same gain. As an example, we consider a FRA pumped by six coherent pumps or two incoherent pumps. Comparison of power transients in those two FRAs is given. It is shown that power transient behaviors of surviving signal channels are almost the same for a FRA pumped by six coherent pumps or two incoherent pumps. However, a FRA with incoherent pumping suffers from slightly severer power transients than that with multiple coherent pumps.

Acknowledgements

I am deeply grateful to my supervisor **Dr. John X Zhang** for his support and guidance, his teaching and inspiration in all phases of this research work. Many thanks and appreciation is due to my family and friends for their encouragement and support.

TABLE OF CONTENTS

LIST OF FIGURES

Acronyms

ASE	amplified spontaneous emission
FRAs	fiber Raman amplifiers
DRB	double-Rayleigh backscattering
DWDM	dense wavelength division multiplexing
EDFA	erbium-doped fiber amplifier
FWHM	full-width at half-maximum
MPI	multiple-path interference
NF	noise figure
OSNR	optical signal to noise ratio
SBS	stimulated Brillouin scattering
SMF	standard single-mode fiber
SNR	signal-to-noise ratio
SRS	stimulated Raman scattering
WDM	wavelength division multiplexing
TW Reach	truewave Reach fiber
RK4	the fourth-order Runge-Kutta
FWM	four-wave-mixing

Chapter 1 Introduction

Rapid growth of communication traffic and the development of high-power compact semiconductor LD pumps have boosted the research on fiber Raman amplifiers. By proper selection of wavelengths and powers of pump sources, fiber Raman amplifiers (FRAs) can exhibit wide amplification bandwidth and flexible center wavelength in comparison with erbium-doped fiber amplifiers (EDFAs).

Wavelength division multiplexing (WDM) technology employing fiber amplifiers provides a platform for significant improvement in network bandwidth capacity. Fast signal power transients caused by cross-gain saturation effects pose a serious limitation in amplified WDM transmission networks. Because optical amplifiers saturate on a total-power basis, addition or removal of channels in a wavelength routing multi-access WDM network will tend to perturb channels at other wavelengths that share all or part of the route. Network reconfiguration and addition/removal of wavelength channels in fiber amplifier will induce power transients in the surviving channels that can cause serious service impairment.

This thesis analyzed transient effects caused by input power fluctuations in fiber Raman amplifiers.

First the overview of Raman amplification in fiber communication systems is described briefly in Section 1.1. The issues treated in this work are then presented Section 1.2. Section 1.3 finally describes the structure of the thesis.

1.1 Overview of Raman amplification in fiber communication systems

In the early 1970s, Stolen and Ippen demonstrated Raman amplification in optical fibers. However, throughout the 1970s and the first half of the 1980s, fiber Raman amplifiers remained primarily laboratory curiosities. In the mid-1980s, many research papers elucidated the promise of fiber Raman amplifiers, but much of that work was overtaken by erbium-doped fiber amplifiers by the late 1980s [1]. However, in the mid- to late 1990s, there was a resurged interest in Raman amplification. Optical amplifiers have played a critical role in the telecommunications revolution that began in the early 1990s. For the first time, lightwave communication systems using inline amplifiers could operate over multiple fiber spans without expensive electronic regeneration. In the mid- to late 1990s, commercial systems exploited this broad bandwidth by wavelength-division multiplexing tens of signal channels together to achieve capacities of hundreds of gigabits per second. Research on Raman amplification in optical fibers started early in the 1970s. By the early part of 2000s, almost every long-haul (typically defined 300 to 800 km) or ultralong-haul (typically defined above 800 km) fiber-optic transmission system uses Raman amplification. The benefits from Raman amplification in the transmission fiber were already being investigated in the mid–1980s. However, Raman gain requires more pump power, roughly tens of milliwatts per dB of gain, as compared to the tenths of a milliwatt per dB required by EDFAs for small signal powers. This disadvantage, combined with the scarcity of high power pumps at appropriate wavelengths, meant that Raman amplifier research subsided during the commercialization of EDFAs in the early 1990s. Then, in the mid-1990s, the development of suitable high power pumps [2] sparked renewed interest. Researchers

were quick to demonstrate some of the advantages that Raman amplifiers have over EDFAs, particularly when the transmission fiber itself is turned into a Raman amplifier, a number of technologies contributed to these advances: dispersion management, higher modulation rates, fiber engineering, forward-error correction, and advanced modulation formats. Raman amplification is an accepted technique for enhancing system performance now.

1.2 Thesis work

The work presented in this thesis investigates transient effects caused by channel addition/removal by simulation in fiber Raman amplifiers. The simulations are based on application of a large signal numerical model which incorporates time variation effects, downstream propagation of multiple signals, upstream propagation of pump and both downstream and upstream propagation of amplified spontaneous emission (ASE). System of coupled non-linear differential equations describing the propagation of the signal, pump and ASE waves along the FRAs and their evolution in time represents a two-boundary value problem. Due to the backward propagating ASE and counter-directional pumping, an iterative forward and backward solution of propagation equations must be used in order to achieve a steady-state distribution of signals, pumps, and ASE powers along the FRAs. We have used the fourth-order Runge–Kutta (RK4) routine, to obtain the steady-state optical power distribution along the fiber. Direct integration is used to obtain time evolution of optical powers as a response to channel addition/removal. Stability of the numerical solution depends on the relation of discretization steps in space and time. Using the numerical model, we investigated output power fluctuations caused by dropping/adding signals in FRAs. We compare the transient results caused by channel

addition/removal in the way both coherent pump and incoherent pump. The effect of pumping scheme, input signal power, pump power, the length and type of Raman fiber, and number of added/dropped channels on the dynamics of surviving channel power fluctuations has been studied. The time evolution of output signal was recorded.

1.3 Thesis structure

The structure of the thesis is described in this section - for each chapter the main contents are described.

In Chapter 2, the theory and the model about Raman amplification process are described. First, origin of Raman scattering is presented in Section 2.1. Raman gain spectrum and Raman amplification in optical fibers are presented in Section 2.2. How to get the general Raman amplifier model is presented in Section 2.3.

In Chapter 3, Raman amplifier characteristics are presented. How to get broad bandwidth amplification is presented in Section 3.1. How to produce some noise sources and their characteristics is presented in Section 3.2. We describe the concept of noise figure in Section 3.3. Raman saturation characteristic is presented in Section 3.4. Since fiber Raman amplifiers saturate on a total-power basis, addition/removal of channels in a WDM causes power transients in surviving channels.

In Chapter 4, the transient effects in fiber Raman amplifiers caused by channel addition/removal are analyzed by coherent pumping. Basic equations and their calculation methods are explained in detail and presented in Section 4.1. Transient effects in fiber Raman amplifiers caused by input power fluctuations have been reported and the effect of pumping scheme, pump power, the length and type of Raman fiber, and number

of added/dropped channels on the dynamics of surviving channel power fluctuations has been studied and presented in Section 4.2, 4.3 and 4.4.

In Chapter 5, fiber Raman amplifier steady state analysis with multiple coherent pumps is presented in Section 5.1. Surviving channel power transient effects by multiple coherent pumps are presented in Section 5.2.

In Chapter 6, fiber Raman amplifier characteristics with multiple incoherent pumps are presented in Section 6.1. Fiber Raman amplifier steady state analysis with multiple incoherent pumps is presented in Section 6.2. Surviving channel power transient effects by multiple incoherent pumps are presented in Section 6.3. Comparison of power transients in fiber Raman amplifiers with multiple coherent pumping or incoherent pumping is presented in Section 6.4.

In Chapter 7, concludes this thesis and summarizes all the results in all previous chapters.

Chapter 2 Fiber Raman Amplifier Theory

In Chapter 2, Raman amplification by stimulated Raman scattering and this process in optical fibers from a phenomenological perspective are presented in Section 2.1. Raman gain spectrum and Raman amplification process in fiber Raman amplifiers are presented in Section 2.2. The Raman propagation equation in both co-propagation and counter-propagation, which includes effects due to group velocity, Rayleigh backscattering, fiber loss, as well as Stokes and anti-Stokes spontaneous emission is presented in Section 2.3. Equations to describe the process of Raman amplification in single-mode optical fiber and Stokes and anti-Stokes spontaneous emission generation with conservation of photon number are derived from first principles. The equation conserves photon number in all modes.

2.1 Origin of Raman scattering

Raman scattering is a shift in the frequency of scattered light due to interaction of the incident light with high-frequency vibration modes of a transparent material. When an optical field is incident on a molecule, the bound electrons oscillate at the optical frequency. This induced oscillating dipole moment produces optical radiation at the same frequency, with a phase shift that leads to the medium's refractive index. Simultaneously, the molecular structure itself is oscillating at the frequencies of various molecular vibrations. Therefore, the induced oscillating dipole moment also contains the sum and

difference frequency terms between the optical and vibration frequencies. These terms give rise to Raman scattered light in the re-radiated field.

Optical photons are scattered by quantized molecular vibrations called optical phonons [3]. Photon energy is lost (the molecular lattice is heated) or gained (the lattice is cooled), shifting the frequency of the light. The meaning of Stokes line is the components of scattered light that are shifted to lower frequencies; those shifted to higher frequencies, anti-Stokes lines. The frequency shift is equal to the oscillation frequency of the lattice phonon that is created or annihilated. Raman scattering can occur in all materials, but in silica glass the dominant Raman lines are due to the bending motion of the Si-O-Si bond (see Figure2.1).

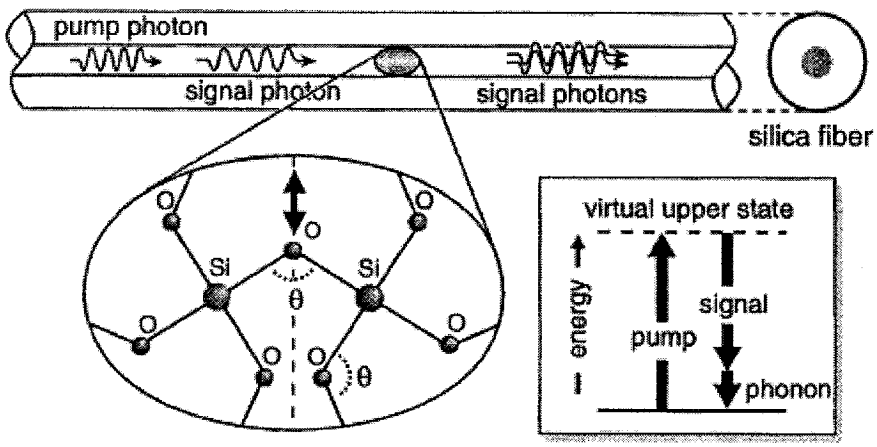

Figure 2.1 The Raman Stokes interaction between a pump and signal photon and the silica molecules converts the pump into a replica of the signal photon, producing an optical photon [3].

Raman scattering can also be stimulated by signal light at an appropriate frequency shift from a pump, leading to stimulated Raman scattering (SRS). Raman process is a process by which pump and signal light are coherently coupled. A pump photon is converted into a second signal photon that is an exact replica of the first, and the

remaining energy produces an optical phonon. The initial signal photon, therefore, has been amplified. Because the upper state is a short-lived virtual state, this process is considered to be nonresonant. In its simplest form, the fiber Raman amplifier is an optically pumped optical amplifier in which an optical signal is amplified by the Raman interaction with a strong optical wave at higher frequency called a "pump." The signal can be pumped in either direction. As the signal is tuned with respect to the pump frequency, the gain is found to be maximal at a frequency separation of 13THz between pump and signal. If the signal frequency is higher than the pump, it will suffer nonlinear absorption rather than amplification. The actual gain curve is broad and closely matches the spontaneous Raman scattering spectrum of the glass. Spontaneous Raman scattering will also occur and is the noise in the Raman amplifier.

2.2 Raman gain spectrum and Raman amplification in optical fibers

Raman gain arises from the transfer of power from one optical beam to another that is downshifted in frequency by the energy of an optical phonon. When an incident photon of frequency v_0 is scattered by a molecule exciting one quantum of vibration energy Ω and producing a downshifted scattered photon of frequency $v_s = v_0 - \Omega$. Raman gain has a spectral shape that depends primarily on the frequency separation between a pump and signal, not their absolute frequencies. This follows from energy conservation: their frequency separation must equal the frequency of the optical phonon that is created. Raman gain does not depend on the relative direction of propagation of a pump and signal. The optical branch of the phonon $\omega - \kappa$ diagram is quite flat [3], and so phonons of a given frequency exist with a broad range of momenta. Therefore, momentum conservation is guaranteed irrespective of the relative directions of pump and signal

photons. Raman scattering is a fast process (subpicosecond [4]). Because SRS is nonresonant, there are no long upper-state lifetimes to buffer pump fluctuations as there are, for example, in EDFAs. However, for reasons of efficiency, Raman amplifiers typically consist several kilometers of fiber. Then, a given portion of signal light can pass through many pump fluctuations if the signal and pump propagate in opposite directions, or if they co-propagate at different velocities. This averaging effect can reduce the impact of pump fluctuations. Raman gain is polarization dependent [5]. The peak coupling strength between a pump and signal is approximately an order of magnitude stronger if they are copolarized than if they are orthogonally polarized.

The Raman gain spectrum in fused silica fibers is illustrated in Figure.2.2 [5]. The gain bandwidth is over 42 THz wide, with the dominant peak near 13.2 THz. The gain band shifts with the pump spectrum, and the peak value of the gain coefficient is inversely proportional to the pump wavelength. The copolarized gain is almost an order of magnitude larger than the orthogonal polarization gain near the peak of the Raman curve. Nonetheless, a polarization-independent Raman amplifier can be made by using polarization diversity pumping to avoid polarization dependent loss. Furthermore, the mixture of modes in a nonpolarization-maintaining fiber helps to scramble the polarization dependence. Raman amplifiers have some fundamental advantages. First, Raman gain exists in every fiber, which provides a cost-effective means of upgrading from the terminal ends. Second, the gain is nonresonant, which means that gain is available over the entire transparency region of the fiber ranging from approximately 0.3 to 2 m. A third advantage of Raman amplifiers is that the gain spectrum can be tailored by adjusting the pump wavelengths. For instance, multiple pump lines can be used to

increase the optical bandwidth, and the pump distribution determines the gain flatness. Another advantage of Raman amplification is that it is a relatively broad-band amplifier with a bandwidth 5 THz, and the gain is reasonably flat over a wide wavelength range. However, a number of challenges for Raman amplifiers prevented their earlier adoption. First, compared to the EDFAs, Raman amplifiers have relatively poor pumping efficiency at lower signal powers. Although a disadvantage, this lack of pump efficiency also makes gain clamping easier in Raman amplifiers. Second, Fiber Raman amplifiers require a longer gain fiber. However, this disadvantage can be mitigated by combining gain and the dispersion compensation in a single fiber. A third disadvantage of fiber Raman amplifiers is a fast response time, which gives rise to new sources of noise, as further discussed below. Finally, there are concerns of nonlinear penalty in the amplifier for the WDM signal channels. Despite these challenges, there has been a revived interest in fiber Raman amplifiers. Several technological advances over the last few years have made Raman amplifiers feasible and practical. It is interesting to note that the physics of Raman has not changed, but rather it is new technologies that have enabled Raman amplifiers to come of age. The first key development has been the availability of higher Raman gain fibers with relatively low loss. As an example, there is more than a tenfold increase in gain efficiency in commercial dispersion compensating fiber compared to standard single-mode fiber (SMF). Moreover, new Raman gain fibers continue to be introduced commercially with different dispersion profiles and dispersion slopes. A second key development for Raman amplifiers has been the availability of high pump power laser diodes or cladding-pump fiber lasers. Cladding-pump fiber lasers are available with output powers 10 W in a SMF. Commercial laser diodes are available with

more than 300-mW output powers, and they will soon to be upgraded to 400 mW [6]. In addition, research on high-power laser diodes shows the availability of output powers in excess of one watt in SMFs in the near future [7]. A third technological development important for Raman amplifiers has been the availability of all fiber components to replace bulk optics. For example, gratings, specialty couplers, wavelength-division multiplexers (WDMs), are now available for splicing easily into all fiber configurations. In addition, fiber-pigtailed bulk-optic couplers are also now commercially available with full high-power reliability qualification mainly based on epoxy-free technologies. A spliced-together fiber amplifier configuration is much more resistant to environmental disturbances than its bulk-optical counterpart. Thus, an up to 100-fold increase in pump power combined with up to a ten-fold increase in Raman gain coefficient leads to a renewed interest in Raman amplification in an all-fiber configuration.

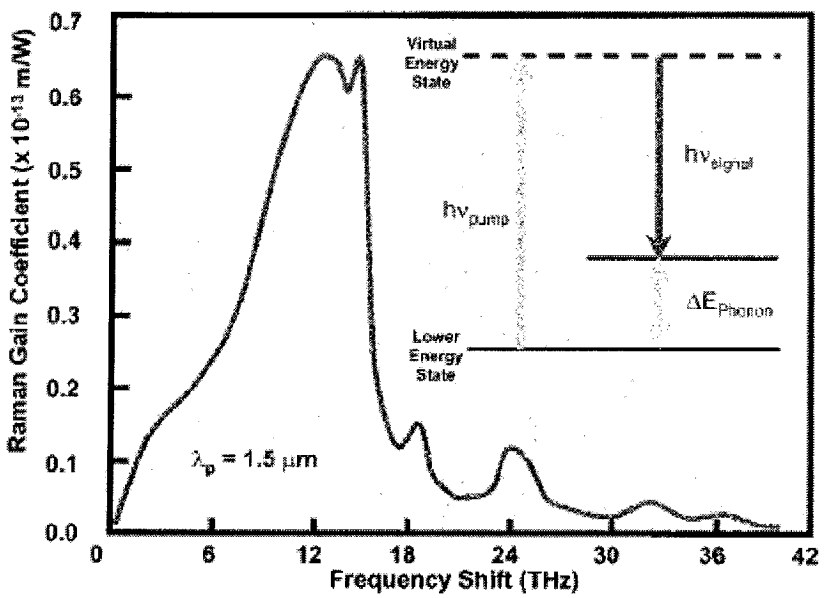

Figure 2.2 Raman gain curve in fused silica fiber for copolarized pump and signal beams. Inset shows an energy level diagram representative of the Raman process, which takes a

higher energy pump photon and splits it into a lower energy signal photon and a phonon [5].

Stimulated Raman scattering is also observed in fibers and in samples placed outside a laser cavity where there are no mirrors to provide feedback. In this single-pass configuration, spontaneous scattered Stokes light is amplified to produce a stimulated Raman output. The fiber is divided into segments of length dz. In each segment the Stokes power increases by spontaneous scattering in the segment and amplification of the Stokes power from all previous segments. There is no input at the Stokes frequency; all the Stokes output is from amplified spontaneous emission.

$$dN_S = dzG(1+N_S)P_0 / A_{eff} \tag{2.1}$$

N_S is the Stokes photon number in the fiber mode per unit frequency bandwidth; G is the gain coefficient; P_0 is the pump power; and A_{eff} is the effective area. To bring out essential features, loss has been neglected. This can be included by replacing the fiber length L with an effective length. The thermal occupation number of the vibration mode is also neglected. This contribution is small at the peak of the Raman gain curve near 13THz. Integration over the length L gives a net Stokes output of

$$N_S(L) = [1 - e^{-GP_0L/A_{eff}}]e^{GP_0L/A_{eff}} \tag{2.2}$$

The quantity in the brackets is an effective input power N_S (noise) that for reasonably large amplification becomes 1.0. Thus the spontaneous scattering along the fiber has been reduced to an effective input of one photon per mode at the Stokes frequency.

The total Stokes power is then an internal over all frequencies and a threshold or critical power is defined where the Stokes power equals the pump power. The condition for a critical power becomes:

$$\frac{GP_0(crit)L}{A_{eff}} = 16 \tag{2.3}$$

Our primary interest is in Raman gain and its associated noise for application in fiber Raman amplifiers. If there is a Stokes signal input $N_S(0)$, the signal amplification and amplified noise will be:

$$N_S(L) = [N_S(0) + N_S(noise)]e^{GP_0L/A_{eff}} \tag{2.4}$$

The power over frequency bandwidth Δv is:

$$P_S = hv_S \Delta v N_S \tag{2.5}$$

So (2.4) becomes:

$$P_S(L) = [P_S(0) + hv_S \Delta v N_S(noise)]e^{GP_0L/A_{eff}} \tag{2.6}$$

If the loss at the signal and pump wavelengths is included (2.4) becomes:

$$P_S(L) = [P_S(0) + hv_S \Delta v N_S(noise)]e^{GP_0L/A_{eff}} / A_{eff} e^{-\alpha_S L} \tag{2.7}$$

Where α_S and α_P are the loss coefficients of the signal and pump wavelengths. The effective length is:

$$L_{eff} = \frac{1 - e^{-\alpha_P L}}{\alpha_P} \tag{2.8}$$

2.3 General model

This section describes the general Raman amplifier model that describes the steady state propagation of signals, pumps and ASE. The Raman interaction between two arbitrary bands with infinitesimal bandwidth Δv and with single-mode polarized light in both bands is considered. We will refer the longer wavelength band as the signal and the shorter wavelength band as the pump. The Raman interaction between the two wavelengths is described by two physical processes [8]. The first process is responsible

for Raman gain and Stokes spontaneous emission generation as well as pump depletion. It is referred to here as the Raman emission process. High signal powers may lead to a depletion of the pump as all the energy is transferred to the signals by the stimulated emission. The second process is responsible for anti-Stokes spontaneous emission generation. It is referred to here as Raman absorption. Raman emission generates a signal photon and a phonon at a frequency that is the difference between the pump and signal frequencies from a pump photon. This process has a rate of $W_{em} = \rho_{em}\left|\left\langle n_p - 1; n_s + 1; n_v + 1 \middle| \alpha_p \alpha_s^+ \alpha_v^+ \middle| n_p; n_s; n_v \right\rangle\right|^2 = \rho_{em} n_p (n_s + 1)(n_v + 1)$, where n_p and n_s are the photon densities at the pump and signal frequencies within the bandwidth Δv, respectively, n_v is the number of phonons at the frequency that is the difference between the pump and signal frequencies, α is the annihilation operator, and α^+ is the creation operator with subscripts describing pump, signal, and phonons. ρ_{em} is a polarization as well as frequency-dependent emission probability coefficient, that will be related later to the Raman gain coefficient.

A process where a signal photon and a phonon combine to produce a photon at the pump frequency is referred to as Raman absorption, with a rate of $W_{abs} = \rho_{abs}\left|\left\langle n_p + 1; n_s - 1; n_v - 1 \middle| \alpha_p^+ \alpha_s \alpha_v \middle| n_p; n_s; n_v \right\rangle\right|^2 = \rho_{abs}(n_p + 1) n_s n_v$, where ρ_{abs} is some frequency and polarization-dependent absorption probability coefficient that will be related later to the Raman gain coefficient. The rate equation for the pump and signal photons can be written as

$$\frac{dn_s}{dt} = -\frac{dn_p}{dt} = W_{em} - W_{abs} \tag{2.9}$$

Using the values for W_{em} and W_{abs} , this equation can be written as propagation equation

$$\frac{dn_s}{dz} = -\frac{V_p}{V_s}\frac{dn_p}{dz} = \frac{\rho_{em}}{V_s} n_p(n_s+1)(n_v+1) - \frac{\rho_{abs}}{V_s}(n_p+1)n_s n_v \qquad (2.10)$$

where V is the group velocity of pump or signal, denoted by the subscript. Converting (2.10) from photon number to power density equations for the depolarized pump and signal

$$\frac{dp_s}{dz} = \frac{g_{0,0}^{eff}(v_p,v_s)}{A_{0,0}^{eff}(v_p,v_s)}\frac{v_p}{v_s} p_p p_s \Delta v + 2hv_s \frac{g_{0,0}^{eff}(v_p,v_s)}{A_{0,0}^{eff}(v_p,v_s)} \times p_p\left(1+\frac{1}{e^{\frac{h(v_P-v_S)}{kT}}-1}\right)\Delta v$$
$$-2p_s\sum_n hv_p \frac{g_{0,n}^{eff}(v_p,v_s)}{A_{eff}^{0,n}(v_p,v_s)}\frac{1}{e^{\frac{h(v_P-v_S)}{kT}}-1}\Delta v \qquad (2.11)$$

$$\frac{V_p}{V_s}\frac{dp_p}{dz} = \frac{g_{0,0}^{eff}(v_p,v_s)}{A_{0,0}^{eff}(v_p,v_s)}\frac{v_p}{v_s} p_p p_s \Delta v - 2hv_p \Delta v \frac{v_p}{v_s}\frac{g_{0,0}^{eff}(v_p,v_s)}{A_{0,0}^{eff}(v_p,v_s)}\left(1+\frac{1}{e^{\frac{h(v_P-v_S)}{kT}}-1}\right)$$
$$+2p_s hv_p \Delta v \frac{v_p}{v_s}\frac{g_{0,n}^{eff}(v_p,v_s)}{A_{eff}^{0,n}(v_p,v_s)}\frac{1}{e^{\frac{h(v_P-v_S)}{kT}}-1} \qquad (2.12)$$

where h is Planck's constant; k is the Boltzmann constant; T is the temperature; v_p and v_s are the pump and signal frequencies, respectively, and g and A_{eff} are the Raman gain and the fiber effective areas, respectively, which are defined in [8]. v_p is always taken to be the highest of the two frequencies. The summation over n in (2.11) and (2.12) represents the spontaneous emission into all modes of the fiber, including radiation modes or a continuous spectrum that is not supported by the fiber, for which case the summation becomes integration. Each mode is considered to have two polarization states and P denotes optical power within bandwidth Δv in both states, with unit of watts per

hertz. In the derivation of (2.11) and (2.12), it is assumed that 1) the phonons obey the Bose–Einstein distribution and are local, because at optical frequencies they cannot efficiently propagate through glass; 2) spontaneous events occur in two polarization states, thus additional factors of two for the second and third term in (2.11) and (2.12); and 3) $\rho_{em} = \rho_{abs}$. The last assumption is justified because if $\rho_{em} \neq \rho_{abs}$, the Raman gain is temperature-dependent. In [9], the Raman gain is independent of temperature is shown between 77 K and 300 K, which justifies the assumption.

Some of the terms in (2.11) and (2.12) are the result of photon number conservation. These are the second terms in (2.11) and (2.12). The contribution due to conservation of photon number can be seen as a temperature and wavelength-dependent loss, but it is not power-dependent. This contribution is the loss present in the fiber due to the conversion of signal and pump photons into spontaneously emitted Raman frequency shifted photons. As presented in (2.11) and (2.12), these terms represent only interaction between the two wavelength bands under consideration, thus, these equations cannot be used directly and should be integrated over all other wavelengths. The third term in (2.11) and (2.12) is responsible for the addition of spontaneously emitted photons at the signal and pump wavelength into the fundamental mode.

Equations (2.11) and (2.12) are extended for the multi-wavelength case and combined to form one general equation, in which multiple channels with optical bandwidths $\Delta\nu$ are included in the co-direction and counter-direction. Here, the channels should cover all the bandwidth under investigation, which includes the bands where only ASE is generated and no signals are present.

$$\pm\frac{dp_i^{\pm}}{dz}=-\alpha(v_i,T)p_i^{\pm}+\gamma(v_i)p_i^{\mp}+p_i^{\pm}\sum_j^{v_j>v_i}\frac{g_{eff}(v_j,v_i)}{A_{eff}(v_j,v_i)}(p_j^{+}+p_j^{-})\Delta v+$$
$$2\sum_j^{v_j>v_i}(p_j^{+}+p_j^{-})hv_i\Delta v\frac{g_{eff}(v_j,v_i)}{A_{eff}(v_j,v_i)}\times(1+\frac{1}{e^{\frac{h(v_j-v_i)}{kT}}-1})$$
$$-p_i^{\pm}\sum_j^{v_j<v_i}\frac{V_j}{V_i}\frac{v_i}{v_j}\frac{g_{eff}(v_i,v_j)}{A_{eff}(v_i,v_j)}(p_j^{+}+p_j^{-})\Delta v+ \tag{2.13}$$
$$2\sum_j^{v_j<v_i}(p_j^{+}+p_j^{-})hv_i\Delta v\frac{v_i}{v_j}\frac{V_j}{V_i}\times\frac{g_{eff}(v_i,v_j)}{A_{eff}(v_i,v_j)}\frac{1}{e^{\frac{h(v_i-v_j)}{kT}}-1}$$

Where i the subscript represents the i th wavelength, the superscripts of + and - represent the co-direction and counter-direction, respectively, α and γ are the wavelength-dependent loss and Rayleigh backscattering coefficients, respectively [10]. In (2.13), α includes the loss due to Raman emissions into all modes, as is usually measured, which means the corresponding terms in (4) are included in α . If needed, the sums over the frequencies can be converted into integrals for a continuous spectrum.

Compared with current data rates, the energy from the Raman pumps is transferred almost instantaneously to the signals, such that the gain experienced by those signals can be calculated from the instantaneous pump power at a given point in the fiber. If there are significant low-frequency data or large numbers of channels are suddenly added or dropped in a dense wavelength division multiplexing (DWDM) system, large power transients may happen. In these cases, the effect of dispersion would be important for co-pumped amplifiers, and the effective fiber length would be important for counter-pumped amplifiers. First, it is very easy for high signal powers that lead to a depletion of the pump as all the energy is transferred to the signals by the stimulated emission. Second, a numerical model can also take account of multiple pumps, which can be used to flatten the gain spectrum. Finally, both signals and pumps will transfer energy among

themselves and this effect is shown to become much stronger as the pump wavelengths become separated and longer wavelength pumps fall into the gain bandwidth of shorter wavelength pumps.

When the Raman pump and signal are co-propagating, the pump power will be strongest at the start of the fiber resulting in a large amount of gain. Because of fiber attenuation at the pump wavelength, the power of the pump will be reduced by fiber attenuation that resulted in a gradual reduction in gain. Eventually the fiber loss will dominate the signal profile. There is little pump power at the start of the fiber with a counter-pumped configuration and the signal undergoes linear loss from the fiber attenuation. The pump power from the end of the fiber becomes progressively stronger such that the signal experiences gain in the last part of the fiber. As this attenuation is increased, the gain becomes concentrated towards the ends of the fiber and the excursions of the signal profile become wider.

Chapter 3 Fiber Raman Amplification Characteristics

In Chapter 3, fiber Raman amplifier characteristics are presented. How to get broad bandwidth amplification is presented in Section 3.1. Fiber Raman amplifiers can have a broad continuum spectrum by multiple pumps. Using this broad-band pumping approach, amplifiers can have gain bandwidths greater than 100 nm. There are four primary sources of noise in Raman amplifiers. How and why to produce these noises and their characteristics is demonstrated in Section 3.2. The Section 3.3 defines an optical amplifier's noise figure (NF) that quantifies how much the amplifier degrades a signal's signal-to-noise ratio (SNR) when the signal is amplified. Raman saturation characteristic is demonstrated in Section 3.4. Since fiber Raman amplifiers saturate on a total-power basis, addition/removal of channels in a WDM causes power transients in surviving channels.

3.1 Broad band amplification using multiple pumps

In optical fiber, the optical phonon shows a broad continuum spectrum. Therefore, we can get the Raman gain spectrum that is already broad over 10-20nm in the 1550nm signal wavelength range generated by one frequency of pump light. As a result, in WDM pumping, each Raman gain caused by each frequency of pump light typically overlaps the other. Therefore, one signal frequency will receive a sum of the overlapped gains from the different pump frequencies. The spectral flexibility of Raman amplification allows the gain spectrum to be shaped by combining multiple pump wavelengths to make

the broad gain bandwidth. Many approaches searching for optimization approaches are studied and give the flattest gain with the fewest number of pumps [11]. One convenient way to design a broadband Raman amplifier is: determination of pump wavelengths, followed by estimation of how much pump power is necessary for each pump wavelength, and finally configuration of passive combiners. We can iteratively but easily determine an optimum set of pump wavelengths by superposition rule. One we choose a set of pump wavelengths, a composite logarithmic Raman gain is thus easily obtained through simply summing each logarithmic Raman gain. Adjusting the weighting factors, we can see possible composite gain spectra for the given set of pump wavelengths to find the desired shape. Amplifiers with gain bandwidths greater than 100 nm have been demonstrated by using this broad-band pumping approach [12]. One must consider the strong Raman interaction between the pumps to design such broad-band Raman amplifiers [13]. The short wavelength pumps amplify the longer wavelengths, and so more power is typically needed at the shortest wavelengths (see Figure 3.1). The noise properties of broad-band amplifiers can be affected by this interaction between the pumps.

The Raman gain spectrum in optical fiber usually has an asymmetric shape around the peak: it has a steeper slope on the high frequency side of the peak. If we try to realize a flat-top spectral shape using WDM pumping and the superposition rule, we should compose the equal-degree but opposite slopes to be added to each other. Because of its asymmetric shape, we need to prepare a number of tiny Raman gain curves slightly shifted from each other to make up a smooth slope opposite to the slope that appears on the low-frequency side of the peak in a gain curve caused by a single pump frequency. The asymmetry of the Raman gain efficiency spectrum means that gain at the longest

signal wavelengths is determined primarily by the location of the longest wavelength pump, even though the shorter wavelength pumps amplify these pumps. The shorter wavelength signals can receive gain contributions more uniformly from several pumps. This is shown in Figure 3.1, where each pump can contribute to gain shown as dashed lines. All these contributions add to give the total broad-band gain (solid line). Even though we launched only 10% of the total pump power at 1495 nm, it is amplified by the other pumps, leading to 80% of the gain for the longest signal wavelengths. Using more than 10 pump wavelengths, we achieve gain flatness less than 0.1dB.

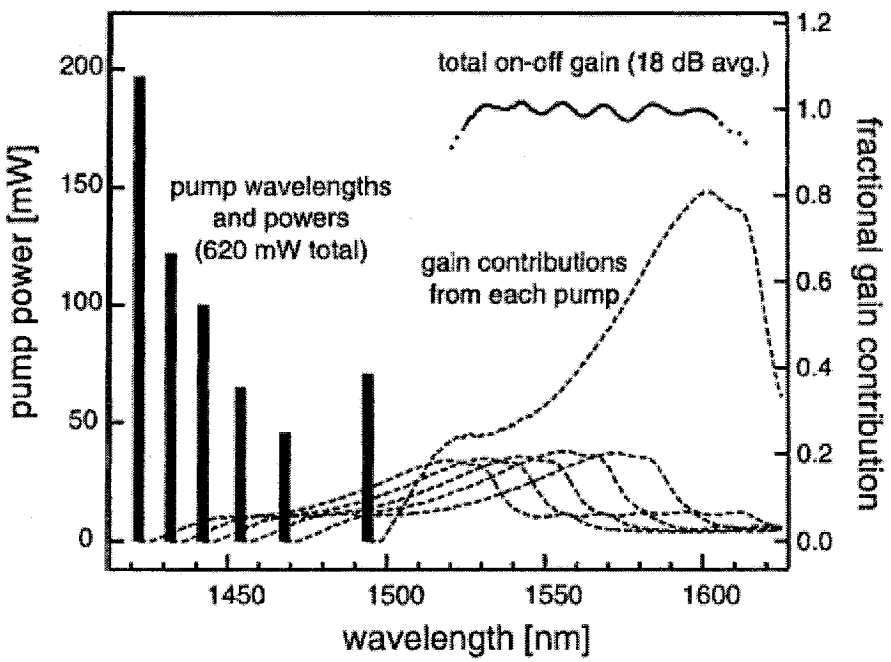

Figure 3.1 Numerical example of broad-band Raman gain obtained using a broad pump spectrum to pump a NZDF. Bars show the counter-pump wavelengths and input powers. Solid line shows the total small-signal on-off gain. Dashed lines show the fractional gain contribution from each pump wavelength [13].

3.2 Noise sources in fiber Raman amplifiers

There are four primary sources of noise in Raman amplifiers. The first is double Rayleigh scattering (DRS) that corresponds to one backward and the other forward scattering events due to the microscopic glass composition nonuniformity. Amplified spontaneous emission (ASE) traveling in the backward direction will be reflected in the forward direction by DRS and experiences gain due to stimulated Raman scattering [14]. For example, MPI occurs when there are two reflection sites along a system. A small portion of the signal light can be delayed as it is multiply reflected between these sites. Therefore, there are two types of light present at the receiver: the "straight-through" light with average power, and delayed light with power. Interference between the two converts phases noise to intensity noise [15], [16]. Raman-amplified systems can produce MPI, for example, by discrete reflections at faulty connectors or splices. The amount of MPI can be exacerbated by Raman gain between the reflection sites because the delayed signal is amplified twice when double-passing between each site. Reflection levels in the span will be intolerable if the reflections lie in regions of high Raman gain [17]. This will degrade the signal-to-noise ratio (SNR). Furthermore, The SNR can be lowered by multipath interference of the signal from DRS. DRS is proportional to the length of the fiber and the gain in the fiber, so MPI is particularly important in Raman amplifiers due to the long length of fiber, where lengths of several kilometers are typically required. From a practical viewpoint, DRS limits the gain per stage to approximately 10 to 15 dB. We may get higher gain amplifiers through the use of isolators between the multiple stages of amplification. For example, a 30-dB discrete Raman amplifier has been demonstrated with two stages of amplification and a noise figure less than 5.5 dB [18].

Even if all the discrete reflections within a span are eliminated, there are still distributed reflections from Rayleigh backscattering in the fiber itself. Rayleigh backscattering can occurs when light is elastically reflected by submicron inhomogeneities in a fiber's refractive index that were frozen into the glass when it solidified. This sets a fundamental limit on the maximum amount of distributed Raman gain that can be used before MPI dominates. Gain in discrete Raman amplifiers that typically use several kilometers of fiber to make efficient use of the pump light. It can be limited by the source of MPI. In the case of discrete amplifiers, however, there is more flexibility in the amplifier design, and the growth of DRB may be eliminated by the techniques such as interstage isolation [19].

The second source of noise arises from the short upper-state lifetime of Raman amplification, as short as 3 to 6 fs [20]. This virtually instantaneous gain can lead to a coupling of pump fluctuations to the signal. The usual way of avoiding this deleterious coupling is to make the pump and signal counter-propagating, which has the effect of introducing an effective upper-state lifetime equal to the transit time through the fiber [21]. If co-propagating pumps and signals are to be used, then the pump lasers must be very quiet. That is, they must have a very low so-called relative intensity noise (RIN). Because stimulated Raman scattering is a nonresonant process, it is inherently fast, occurring over subpicosecond time scales [22]. Therefore, pump power fluctuations can be transferred to signals as noise. In fiber amplifiers, because pumps and signals propagate along many kilometers of fiber, they interact over time scales that are considerably longer. This produces an averaging effect that limits the bandwidth over which pump noise is transferred to the signals.

A third primary source of noise in Fiber Raman amplifiers is the usual ASE. In addition to producing gain, Raman amplifiers produce noise. The most important source of noise is amplified spontaneous emission (ASE), which is an unavoidable by-product of gain in all optical amplifiers. In the case of Raman amplifiers, ASE is generated by spontaneous Raman scattering. As the gain becomes large within the amplifier, gain has significant contribution to the forward ASE, from Rayleigh scattered ASE that was traveling in the backward direction. As amplified ASE becomes larger and larger, the amplifier will eventually lase [23]. The Raman effect is a very low noise process, and in most single-channel cases amplification will result in the emission of nearly one spontaneous photon per mode. An ultrabroadband WDM system may have wavelength channels that lie close to Raman pump wavelengths. The reason for the large increase in spontaneous emission at shorter wavelengths can be understood by decomposing the gain spectrum into its constituent components provided by each pump wavelength. Understanding how much is produced is crucial because noise accumulation causes transmitted information to be corrupted. As is typical for reasonable signal power levels, signal–ASE beating noise dominates over ASE–ASE beating noise. Fortunately, Raman amplifiers have inherently low noise from signal–ASE beating because a Raman system always acts as a fully inverted system. For example, the ASE power spectral density can be written as [24]

$$S_{ase}(v) = (G-1)hv(H_2 / N_2 - N_1) \tag{3.1}$$

and the noise figure as

$$NF = 1/G(2S_{ase}(v)/hv + 1) \tag{3.2}$$

Where N_2 is the upper state population and N_1 is the lower state population. For Raman amplifiers, the $N_2/(N_2 - N_1)$ term is always equal to one, whereas in EDFAs it is usually greater than one. In an EDFA, this term is only equal to one for an amplifier fully inverted through the entire length of gain fiber. On the other hand, since Raman amplifiers use long fiber lengths, the small fraction of passive loss of the gain fiber needs to be added to the noise figure. Nonetheless, discrete Raman amplifiers with noise figures as low as 4.2 dB have been reported.

Finally, a fourth source of noise arises from the phonon-stimulated optical noise created when wavelength signals being amplified reside spectrally close to pump wavelengths used for amplification. As the difference between pump and signal frequencies becomes small and therefore the energy difference between the ground and first energy level becomes small, there is an increased probability of finding the glass molecule at the first energy level rather than the ground state. This results in a greater probability of spontaneous emission when the pump photon is incident on the molecule, and therefore a larger amount of spontaneous noise from the amplifier. As the temperature increases, there is a dramatic increase in the amount of spontaneous emission at shorter frequency shifts. In other words, at room or elevated temperatures there is a population of thermally induced phonons in the glass fiber that can spontaneously experience gain from the pumps, thereby creating additional noise for signals close to the pump wavelengths. This effect can lead to an increase in noise figure of up to 3 dB for signals near the pump wavelength [25].

We can describe the noise properties of Raman amplifiers using several quantities. One is the optical signal-to-noise ratio (OSNR). OSNR is defined as the ratio of the

optical signal power to the power of the ASE in a given reference bandwidth (often 0.1 nm) around the signal wavelength. Usually, we include the ASE power in all polarizations, even though only ASE components with the same polarization state as the signal produce beat noise. Therefore, care needs to be taken when using such a definition if the ASE is partially polarized, as can occur if there is polarization-dependent loss or gain. The OSNR can be measured using a number of techniques, such as ASE interpolation, polarization extinction, and time-domain extinction. Each of these interpolates the amount of ASE actually causing beat noise using ASE at different wavelengths or polarizations from the signal, or using ASE produced at different times.

Another important quantity is the electrical signal-to-noise ratio (SNR). This is the ratio of the signal electrical power to the noise power, measured after photodetection. Because the electrical signal power is proportional to the photocurrent squared, the SNR is often defined as i^2/σ_i^2, where σ_i^2 is the photocurrent variance [26]. In general, σ_i^2 depends on the magnitude of the optical signal power; that is, on whether a 1 or 0 bit is being detected. Note that the SNR is sensitive not only to signal-spontaneous beat noise, but to any noise mechanism that increases the photocurrent variance. Unlike the OSNR therefore, which is only relevant for noise generated by ASE, the SNR encompasses all sources of intensity noise.

3. 3 Noise figure

3.3.1 Introduction to noise figure

The concept of noise figure is a well established method of characterizing the buildup of noise in electrical components. It quantifies how much the amplifier degrades a signal's SNR when the signal is amplified. The definition of a noise figure that has been

used for electrical components is the signal-to-noise ratio at the input of a device divided by the signal-to-noise ratio at the output: It is defined as

$$NF = SNR_{in} / SNR_{out} \tag{3.3}$$

It has been the convention in optical communications to define SNR in terms of electrical powers at an ideal receiver and therefore optical powers and noises must be converted to the electrical currents. In the case of optical amplifiers it is assumed that the input signal is as noise free as possible and is only degraded by shot noise resulting from the fundamental particle nature of light. This assumption ensures that NF has the maximum sensitivity to noise added by the amplifier. Furthermore, it is assumed that is measured using an ideal photodetector with a quantum efficiency of 100%.

In a discrete Raman amplifier, the wavelength dependence of the noise figure will be determined by four main factors. These include the gain spectrum and component losses at the amplifier input, SRS interactions between the pump wavelengths, and increased spontaneous emission due to the thermal distribution of phonons in the ground state. When the signal and pump lie close together, the spontaneous emission factor may be large. If the ratio of the gain given by that pump to the overall total gain from all the pumps is small, the noise figure will also tend to 3dB. However, if a pump provides a large amount of gain to the closely spaced signal, there will be a large increase in the excess spontaneous noise.

In the case where signal-spontaneous beat noise is the dominant source of noise added by an optical amplifier, its NF can be approximated in linear units as [25].

$$NF \approx 2P_A^+(L)/hvB_{ref}G_{net} + 1/G_{net} = P_S(0)/hvB_{ref}OSNR_{out} + 1/G_{net} \tag{3.4}$$

The first term corresponds to noise from signal-spontaneous beating and the $1/G_{net}$ term accounts for shot noise. In general, however, NF can also include contributions from other sources of noise such as spontaneous-spontaneous beating or multiple-path interference. In a well controlled amplifier, the MPI term will not be present. However, if this is not the case, it can dominate over other noise terms inasmuch as it is both proportional to the signal power and to the gain of the amplifier. The noise figure is not independent of the signal power even if MPI is ignored. When designing amplifiers, one must typically consider tradeoffs between minimizing signal-spontaneous beating at the expense of increasing other sources of noise.

If several amplifiers are cascaded together, the total noise figure of the amplifier chain is given by [27]

$$NF_{total} = NF_1 + (NF_2 - 1)/G_1 + (NF_3 - 1)/G_1G_2 + \ldots \quad (3.5)$$

where NF_i and G_i are the noise figure and net gain (in linear units) for the i^{th} amplifier in the chain. This shows that the total noise figure is dominated by the noise figure of the first amplifier (NF_1) if its gain (G_1) is sufficiently high. Hence, many high performance optical (and electrical) amplifiers are multistage amplifiers with a low-noise, high-gain first stage, called a preamplifier stage.

3.3.2 Noise figure of distributed Raman amplifiers

The concept of preamplification is crucial for understanding improvements in system performance gained from distributed Raman amplification. As an example, consider a fiber span, 100 km in length that produces 20 dB of signal loss [28] [29]. Without Raman pumping, a negligible amount of ASE is generated within the fiber span, and so the OSNR is not degraded. Therefore, (3.4) shows that the NF of the unpumped

span equals the second term ($1/G_{net}$), which in dB equals the 20-dB span loss. If a discrete amplifier follows the span, the total noise figure for the span-plus-amplifier can be calculated using (3.5), where the first 'amplifier' in the chain is the passive span. Therefore, NF_{total} in linear units, is the span loss multiplied by the noise figure of the discrete amplifier. In dB, if the discrete amplifier NF is 5 dB, NF_{total} is 25 dB. Now, if Raman counter-pumping is added, the signal power follows trajectories like those shown in Figure 3.2 [30] These simulated curves, calculated for on-off gains ranging from 0 dB (pump off) to 20 dB (transparent span), show that Raman pumping effectively converts the last 30 km of fiber into a preamplifier stage. The resulting improvement in NF_{total} for the span plus discrete amplifier is shown in Figure 3.3 [31]. Increasing the on-off Raman gain from 0 to 20 dB, reduces the NF_{total} from 25 to 17.5-dB (solid line). (This improvement is closely related to the increase in the minimum signal power in the span, but they are not equal as is sometimes assumed.) In fact, with 20-dB of on-off gain, NF_{total} is only 0.2-dB higher than the noise figure of the Raman-pumped fiber span, denoted as NF_{span} (dashed line). This shows that high Raman gain effectively "hides" the noise figure of the discrete amplifier.

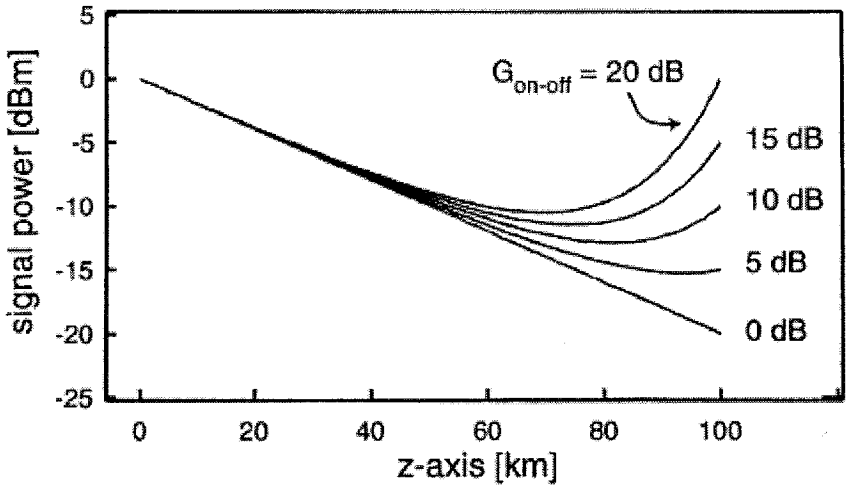

Figure 3.2 Simulation signal power evolution for different values of on-off gain [30].

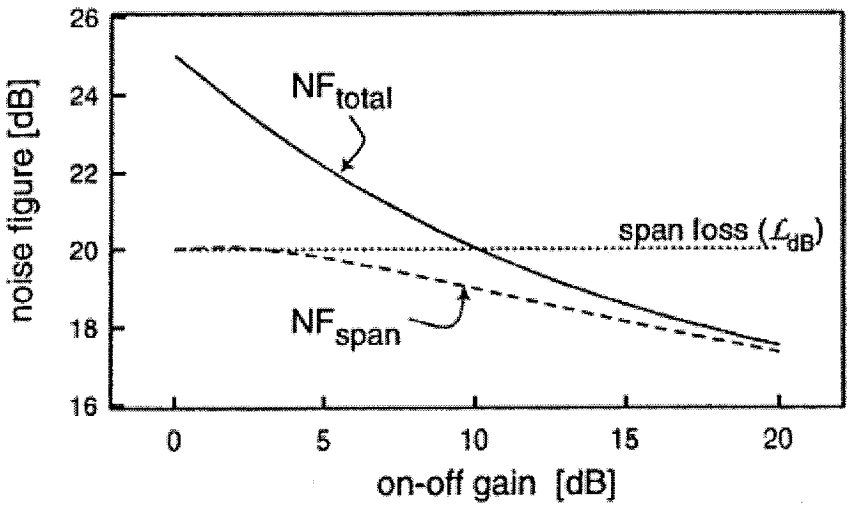

Figure 3.3 Simulated values for NF versus on-off Raman gain. The solid line shows the noise figure of a counter-pumped fiber span plus discrete amplifier with a 5-dB noise figure. Dashed lines show the noise figure of the Raman-pumped fiber span alone. Dotted line indicates the loss of the unpumped span [31].

3.4 Raman amplifier saturation characteristics

Pump depletion leads to gain saturation which also changes the noise figure and normalized path-average power. Pump depletion alters the power distribution inside the

Raman amplifier for a fixed gain and it increases the pump power needed to achieve that gain. In the saturated case more pump power is needed to compensate for the saturation. Saturation in Raman amplifier is very different. The gain medium is very fast and responds almost instantaneously. Running such an amplifier in large degrees of saturation would introduce a lot of inter-channel gain saturation induced crosstalk. The fast gain dynamics also makes it possible to construct gain controlled Raman amplifiers which can react to input power variations in a fraction of a loop round-trip for testing constant signal power systems. For a fixed pump power any increase in signal power will lead to a decrease in gain. It shows that saturation occur sooner and is more pronounced with increased gain. The figure 3.4 also shows that Raman amplifiers have a much more gradual saturation response. The impact of saturation on noise figure increases with pump power (gain). One way to compensate the saturation is to increase the pump power, so that a specific gain maintained. Keeping the gain constant has two applications: (1) In constant signal power systems it would keep the signal power constant down the transmission line compensating for the noise accumulation. (2) In constant total power systems the saturated gain of the first amplifier would be adjusted to match the loss of the span.

Since fiber Raman amplifiers saturate on a total-power basis, addition/removal of channels in a WDM network may disturb channels at other wavelengths that share the same path, causing power transients in surviving channels that could result in serious service impairment.

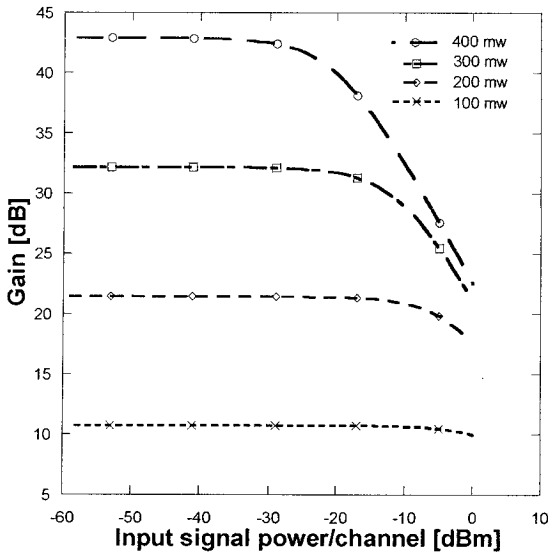

Figure 3.4 Gain versus signal input power for forward pumped 40 km TW Reach fiber Raman amplifiers. Curves corresponding to pump powers of 100 mW, 200 mW, 300 mW, and 400 mW with wavelength 1550 nm are shown.

Chapter 4 Analysis of Fiber Raman Amplifier Transients with One Coherent Pump

We study power transients in fiber Raman amplifiers pumped counter-directionally by coherent pumping in Chapter 4. Transients are defined as the output signal power response to abrupt change in the number of signal channels at the input to fiber Raman amplifiers (channel addition/removal). During the transience, if the signal power increases, the enhanced nonlinearities may distort the signal, while decreased signal power may lead to OSNR impairment; and both effects will degrade the system performance. Transients in Raman amplification is determined by pump-depletion level, the amount of pump-power change seen by the signal. An arbitrary signal channel in DWDM system experiences Raman amplification by all the shorter wavelength channels and Raman depletion by all the longer wavelength channels simultaneously. Hence, the power transfers caused by SRS at channels with the shortest and longest wavelengths are the most profound. Our numerical model of fiber Raman amplifiers is based on the coupled non-linear partial differential equations that include pump-to –pump, pump-to signal, and signal-to-signal Raman interactions, Rayleigh backscattering, wavelength dependent fiber loss, spontaneous emission noise and thermal noise. The surviving channel power fluctuations depend on the position of the dropped/added channels within the flat band of fiber Raman amplifiers. System of coupled non-linear differential equations describing the propagation of the signal, pump and ASE waves along the FRA and their evolution in time represents a two-boundary value problem. Due to the

backward propagating ASE and counter-directional pumping, an iterative forward and backward solution of propagation equations must be used in order to achieve a steady-state distribution of signals, pumps, and ASE powers along the FRA. We have used the fourth-order Runge–Kutta routine, to obtain the steady-state optical power distribution along the fiber. Direct integration is used to obtain time evolution of optical powers as a response to channel addition/removal. Stability of the numerical solution depends on the relation of discretization steps in space and time. Transient effects in fiber Raman amplifiers caused by pumping scheme, input signal power, fiber type, different signal wavelength, pump power, the length of Raman fiber, and the number of added/dropped channels have been simulated in chapter 4 [32]-[38].

4.1 Basic equations, calculation explanation and verification program

4.1.1 Basic equations and calculation explanation

Downstream propagating multiple signal channels are aggregated/distributed via multiplexer/demultiplexer. Multiple pump powers are combined in power combiner and launched into the optical fiber by a fused or dielectric pump coupler. The dynamic model used for the simulation is derived from the steady-state model of Raman fiber amplifier described in (2.13). Generation and propagation of spontaneous emission noise were taken into account. When backward Rayleigh scattering, temperature dependent spontaneous Raman emission and wavelength dependence of fiber loss and group velocity are taken into consideration, the propagation equations for forward and backward propagating pumps, signals, and spectral components of amplified spontaneous emission powers $P^{\pm}(z,v,t)$, describing their evolution along the optical fiber in space and time, acquire the form [37].

$$\frac{\partial P^{\pm}(z,v,t)}{\partial z} \mp \frac{1}{V_g(v)} \frac{\partial P^{\pm}(z,v,t)}{\partial t} =$$

$$\mp\alpha(v)P^{\pm}(z,v,t) \pm \gamma(v)P^{\mp}(z,v,t)$$

$$\pm P^{\pm}(z,v,t) \bullet \sum_{\xi>v} \frac{g_R(v-\xi)}{K_{eff}A_{eff}} \bullet [P^{\pm}(z,\xi,t) + P^{\mp}(z,\xi,t)]$$

$$\pm hv \sum_{\xi>v} \frac{g_R(v-\xi)}{A_{eff}} \bullet [P^{\pm}(z,\xi,t) + P^{\mp}(z,\xi,t)] \bullet [1 + \frac{1}{\exp[h(\xi-v)/kT]-1}]\Delta v$$

$$\mp P^{\pm}(z,v,t) \bullet \sum_{\xi<v} \frac{v}{\xi} \frac{g_R(v-\xi)}{K_{eff}A_{eff}} \bullet [P^{\pm}(z,\xi,t) + P^{\mp}(z,\xi,t)]$$

$$\mp 2hvP^{\pm}(z,v,t) \bullet \sum_{\xi<v} \frac{g_R(v-\xi)}{A_{eff}} \bullet [1 + \frac{1}{\exp[h(v-\xi)/kT]-1}]\Delta v$$

(4.1)

where $V_g(v)$ is the frequency dependent group velocity; $\alpha(v)$ is the fiber background loss; $v(v)$ is the Rayleigh back scattering coefficient; $g_R(v-\xi)$ is the Raman gain coefficient between waves with frequency v and ξ; K_{eff} is the polarization factor between pumps and Stokes signals; A_{eff} is the effective interaction area of the fiber; h is the Planck's constant; k is the Boltzman's constant and T is the absolute temperature of the fiber.

In silica fibers, the region of non-zero Raman gain spans the range of frequencies of about 35 THz; starting from the pump with the highest frequency (lowest wavelength). Boundary conditions imposed on pump, signal, and ASE powers are:

$$P^{+}(z=0,v_P) = P_{P0}^{+}(v_P)$$

$$P^{-}(z=L,v_P) = P_{P0}^{-}(v_P)$$

$$P^{+}(z=0,v_S,t) = P_{P0}^{+}(v_S,t)$$

$$P^{+}(z=0,\nu_{ASE}) = P^{-1}(z=L,\nu_{ASE}) = 0 \qquad (4.2)$$

Where $P^{+}_{P0}(\nu_P)$, $P^{-}_{P0}(\nu_P)$ are the downstream and upstream input pump powers; $P^{+}_{S0}(\nu_S,t)$ is the time variable input signal power; ν_s, ν_p and ν_{ASE} are the frequencies of signals, pumps, and ASE spectral components.

In case of N_P pumps, N_S signal channels and N_{ASE} spectral components of ASE powers, propagation equation (4.1) forms a system of $N_P + N_S + 2N_{ASE}$ coupled non-linear differential equations. Numerical solution to the time dependent system of (4.1) is separated into two steps:

(1) Determination of steady-state distributions of all optical powers along the fiber for continuous wave input signal of all DWDM channels,

(2) Time evolution of steady-state distributions of all optical powers along the fiber when some DWDM channels are periodically dropped/added with repetition frequency. To obtain steady-state power distributions, time derivative in (4.1) is set to zero.

Coupled non-linear differential equations describing the propagation of the signal, pump and ASE waves along the optical fiber represent a two boundary value problem. Due to the backward propagating ASE and upstream pumping, an iterative forward and backward integration of propagation equations must be used. We have used the fourth-order Runge–Kutta routine.

When the RK4 routine is used for numerical integration of (4.1), the optical fiber of length L, is subdivided into M slots of equal width Δz. For the RK4 approach, the iterative solution is started with forward solution, at z = 0, of downstream pumps, signals and ASE powers. The upstream pumps and ASE powers are set to zero at each mesh point along the optical fiber. At each backward integration the results of previous forward

solution $P^+(z=L,v_P)$, $P^+(z=L,v_S)$ and $P^+(z=L,v_{ASE})$ together with boundary conditions $P^-(z=L,v_P)=P_{P0}^-(v_P)$, $P^-(z=L,v_{ASE})$ =0 are used as starting conditions. Similarly, the results of the previous backward solution $P^-(0,v_P)$, $P^-(0,v_S)$ and $P^-(0,v_{ASE})$ together with boundary conditions:

$$P^+(z=0,v_P)=P_{P0}^+(v_P),P^+(z=0,v_S)=P_{S0}^+(v_S),P^+(z=0,v_{ASE})=0$$

are used as starting conditions for each next forward solution. The iteration is stopped when, in two successive forward iterations, output power of a selected DWDM channel $P^+(L,v_S)$ does not change more than 0.01%.

Once the steady-state distribution of forward and backward propagating optical powers is calculated, direct integration according to (4.3) is used to obtain time evolution of individual optical powers $P^{\pm}(z,v,t)$ along the optical fiber in response to channel addition/removal. The time derivative $\partial P^{\pm}(z,v,t)/\partial t$ is eliminated from (4.1).

$$P^{\pm}(z,v,t+\delta t)=P^{\pm}(z,v,t)+\frac{\partial P^{\pm}(z,v,t)}{\partial t}\bullet\Delta t \qquad (4.3)$$

To simulate channel loss/addition, when $kT_m \le t < (k+\frac{1}{2})T_m \quad k=0,1,2,....$

$$P_{S0}^+(v_S,t)=P_{S0}^+(v_s)$$

When $(k+\frac{1}{2})T_m \le t < (k+1)T_m \qquad k=0,1,2,....$

$$P_{S0}^+(v_S,t)=0$$

where $P_{S0}^{+}(v_S)$ is the input power of DWDM signal channel with frequency v_s (see (4.2)). In order to avoid possible oscillations of the solution in the time domain, care must be taken in the selection of bin widths used in the space (Δz) and time (Δt) discretization schemes. We can derive the difference equations as follows (Vg is group velocity).

$$\frac{(P_i)_{k+1}^{n}-(P_i)_{k}^{n}}{\Delta z}-\frac{1}{V_g}\frac{(P_i)_{k}^{n+1}-(P_i)_{k}^{n}}{\Delta t}=f^{-}(P,S), \tag{4.4}$$

$$\frac{(S_j)_{k}^{n}-(S_j)_{k-1}^{n}}{\Delta z}+\frac{1}{V_g}\frac{(S_j)_{k}^{n+1}-(S_j)_{k}^{n}}{\Delta t}=f^{+}(P,S), \tag{4.5}$$

The meaning of (4.4) and (4.5) is as follows. The procedure is discrete in the time domain with step size Δt. The fiber of the amplifier is split into small segments in order to remove position dependency (the total number of segments is K). At time $t=n\Delta t$, the pump power at each node of the fiber is $(P_i)_1^n$,$(P_i)_2^n$,...,$(P_i)_k^n$, $(P_i)_{k+1}^n$, respectively, where $(P_i)_{k+1}^n$ is the pump power injected into the forward end or the back end of the amplifier's fiber at time $t=n\Delta t$, and subscript i denotes the pump at different wavelengths. Similarly, the signal power at each node is $(S_j)_1^n$, $(S_j)_2^n$,...,$(S_j)_k^n$, $(S_j)_{k+1}^n$, where $(S_j)_1^n$ is the signal power injected into the front end of the amplifier's fiber at time $t=n\Delta t$, and subscript j denotes the signal at different wavelengths. During the interval from time $t=n\Delta t$ to time $t=(n+1)\Delta t$, when the signal power is transmitted forward and the pump power is transmitted backward, at the same time there are interactions among them. At time $t=(n+1)\Delta t$, the sequence of pump power becomes $(P_i)_1^{n+1}$, $(P_i)_2^{n+1}$,..., $(P_i)_k^{n+1}$, $(P_i)_{k+1}^{n+1}$. The sequence of signal power is $(S_j)_1^{n+1}$, $(S_j)_2^{n+1}$,..., $(S_j)_k^{n+1}$, $(S_j)_{k+1}^{n+1}$.

The convergence condition of the upwind-format difference equation is $V_g \Delta t \leq \Delta z$ (the Courant–Friedrichs–Lewy condition). Then from (4.4) and (4.5) we can derive

$$(P_i)_k^{n+1} = (P_i)_{k+1}^n + V_g \Delta t \bullet f^-(S,P) \tag{4.6}$$

$$(S_j)_k^{n+1} = (S_j)_{k-1}^n + V_g \Delta t \bullet f^+(S,P) \tag{4.7}$$

The meaning of the difference equations (4.6) and (4.7) is as follows: $(P_i)_k^{n+1}$, the pump power of k^{th} node at time $t = (n+1)\Delta t$ is derived from $(P_i)_{k+1}^n$ (the pump power of the $k+1^{th}$ node at time $t = n\Delta t$ transmitted backward by Δz; and $(S_j)_k^{n+1}$, the signal power of k^{th} node at time $t = (n+1)\Delta t$ is derived from $(S_j)_{k-1}^n$ (the pump power of $k-1^{th}$ node at time $t = n\Delta t$) transmitted forward by Δz.

Starting with the signal power of each node $(S_j)_k^n (k = 1, 2, \ldots K)$ at time $t = n\Delta t$, after calculation, we derive the signal power sequence of each node $(S_j)_k^{n+1} (k = 2, 3, \ldots K+1)$ at time $t = (n+1)\Delta t$. In the sequence, $(S_j)_{k+1}^{n+1}$ is the signal power output from the amplifier at time $t = (n+1)\Delta t$, and $(S_j)_0^{n+1}$ denotes the input-signal power injected into in front end of the fiber, which is available from the known conditions. We can calculate the signal power at the next time step. The pump power, ASE power, and Rayleigh backscattering power can also be calculated following the same algorithm. In brief, we can calculate the power in the amplifier at any time with the available input and initial conditions through recursion. During the calculation, simple algebraic calculations are used rather than the intensive numerical integration. As a finite difference method, the step size: Δz, ($\Delta t = \Delta z / V_g$) in the process of calculation affects the accuracy of calculation result. By reducing the step size, we can get more accurate result we need.

4.1.2 Verification program

To demonstrate the effect of the pumping scheme on surviving channel power transients, we assume that 40 km of TW Reach fiber is pumped co-directionally, pumped counter-directionally, or pumped bi-directionally by $P_p = 550\,\text{mW}$, $\lambda_p = 1450$ nm and the input signal power is 0 dBm/channel. Balanced pumping ($P_p^+ = P_p^- = 275\,\text{mW}$) is considered in case of a bidirectional scheme. The fiber Raman gain medium is TW Reach fiber, which has the following measured parameters: fiber loss changing from 0.4 dB/km at 1262 nm to 0.2 dB/km at 1573 nm with the water peak loss of 0.33 dB/km at 1382 nm, Rayleigh scattering coefficient varying from -33.7 dB/km at 1500 nm to -35.4 dB/km at 1620 nm, effective fiber core area increasing from 46 μm^2 at 1440 nm to 58 μm^2 at 1590 nm, and Raman gain coefficient peaked at 0.608 $(W \cdot km)^{-1}$ with a frequency shift of 13.3 THz measured by pumping at 1460 nm. Figure 4.1 compares output power variations of the surviving channel for the three pumping schemes. For each scheme, the propagation delay τ through the Raman fiber equals to 195.5 μs. We observe surviving channel power fluctuations as a function of time when two input signal channels ($\lambda_s = 1552$ nm, $\lambda_s = 1553$ nm) out of three input signal channels ($\lambda_s = 1550$ nm, $\lambda_s = 1551$ nm, $\lambda_s = 1552$ nm) are dropped at the time t= t_0 =0 μs and added again at the time t=1000 μs. It was shown that calculated power transient behaviors of surviving signal channel for three pumping schemes are very similar to Figure 4.2 [37].

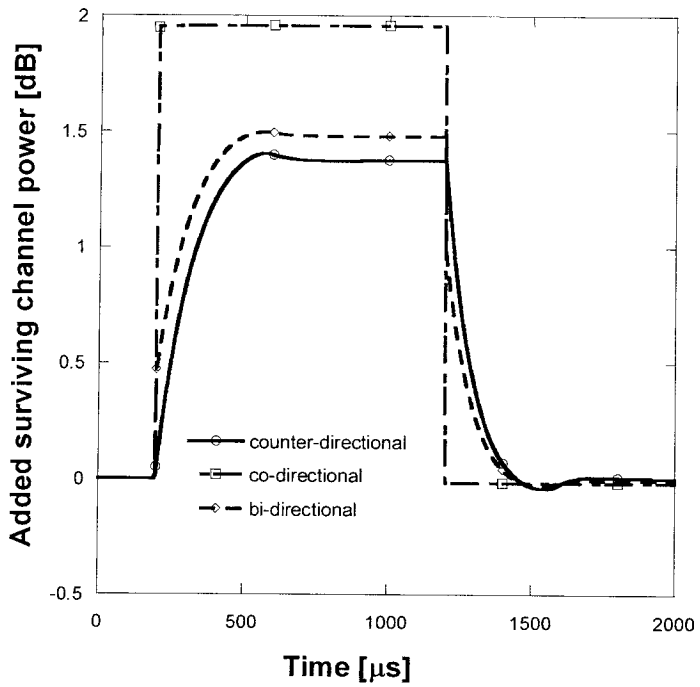

Figure 4.1 Surviving channel power fluctuation as a function of time when two out of three channels are dropped/added-effect of pumping scheme: $L_{TW-Reach}$=40 km; λ_P =1450 nm; P_P=550 mW; λ_s = 1550 , 1551, and 1552 nm; and $P_{s,in}$=0 dBm/channel.

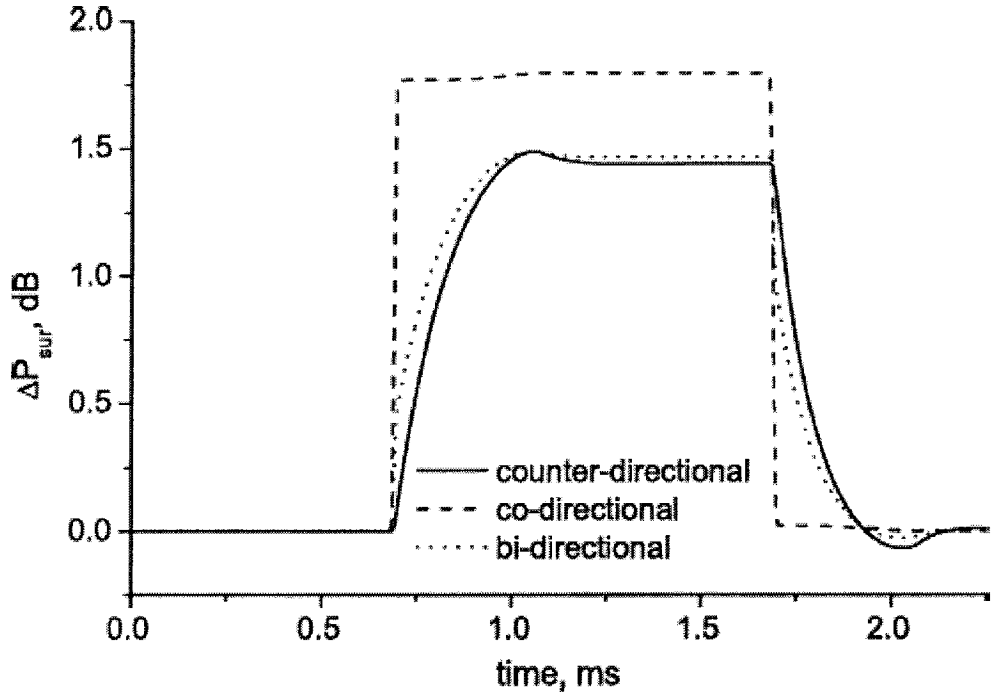

Figure 4.2 Surviving channel power fluctuation as a function of time when two out of three channels are dropped/added-effect of pumping scheme: L_{DS-SMF}=40 km; λ_P =1450 nm; P_P=800 mW; λ_s =1550, 1551, and 1552 nm; and $P_{s,in}$=0 dBm/channel [37].

In the following paragraphs, some results of our numerical simulations of surviving channel power fluctuations due to channel addition/removal will be presented. In these simulations, we have considered Truewave Reach (TW Reach) fiber.

4.2 Surviving channel power transients

4.2.1 Pumping scheme

To demonstrate the effect of the pumping scheme on surviving channel power transients, we assume that 40 km of TW Reach fiber is pumped co-directionally, pumped counter-directionally, or pumped bi-directionally by $P_p = 550$ mW, $\lambda_p = 1450$ nm and the input signal power is 0 dBm/channel. Balanced pumping ($P_p^+ = P_p^- = 275$ mW) is

considered in case of a bidirectional scheme. The fiber Raman gain medium is TW Reach fiber, which has the following measured parameters: fiber loss changing from 0.4 dB/km at 1262 nm to 0.2 dB/km at 1573 nm with the water peak loss of 0.33 dB/km at 1382 nm, Rayleigh scattering coefficient varying from -33.7 dB/km at 1500 nm to -35.4 dB/km at 1620 nm, effective fiber core area increasing from 46 μm^2 at 1440 nm to 58 μm^2 at 1590 nm, and Raman gain coefficient peaked at 0.608 $(W \cdot km)^{-1}$ with a frequency shift of 13.3 THz measured by pumping at 1460 nm. Figure 4.3 compares output power variations of the surviving channel for the three pumping schemes. For each scheme, the propagation delay τ through the Raman fiber equals to 195.5 μs. We observe surviving channel power fluctuations as a function of time when two input signal channels ($\lambda_s = 1552$ nm, $\lambda_s = 1553$ nm) out of four input signal channels ($\lambda_s = 1550$ nm, $\lambda_s = 1551$ nm, $\lambda_s = 1552$ nm, $\lambda_s = 1553$ nm) are dropped at the time t=t_0=0 μs and added again at the time t=1500 μs. In case of bi- and counter-directional pumping, the steady-state power excursion and the speed of power transients are comparable. In case of counter-directional pumping, surviving channel power fluctuation is 0.9298 dB for signal wavelength $\lambda_s = 1550$ nm. In case of bi-pumping, surviving channel power fluctuation is 1.061dB for signal wavelength $\lambda_s = 1550$ nm. In case of co-pumping, surviving channel power fluctuation is 1.507dB for signal wavelength $\lambda_s = 1550$ nm. The rise time (from 10% to 90% of the maximum value) is 158.9 μs and 198.2 μs for bi- and counter-directional schemes, respectively, when surviving channel signal wavelength is $\lambda_s = 1550$ nm. The surviving channel power transient is much faster in the case of co-directional pumping: the rise time is 6.2 μs ;

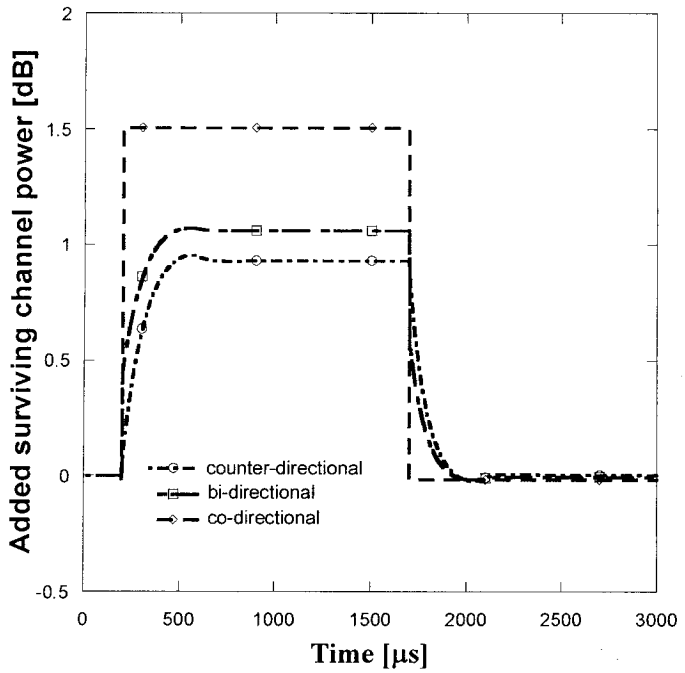

Figure 4.3 Surviving channel (λ_s =1550 nm) power fluctuation as a function of time.

Long rise and fall times of surviving channel power transients in counter- and bi-directionally pumped fiber Raman amplifiers are caused by the fact that signal and pump waves propagate in opposite directions. For the assumed pump and signal powers, the pump power is deeply depleted by the signals along more than 50% of the Raman fiber length, and the cross coupling among the amplified signal channels is significant. Distribution of pump and signal powers along the Raman fiber demonstrating the power depletion is displayed in Figure 4.4 for co- and counter-directional pumping schemes and the case that all four signal channels are on. In the co-directional pumping scheme, pump and signal waves propagate in the same direction with almost equal group velocities. Therefore, after dropping two signal channels, the pump power starts to grow, mainly in the region where it was most depleted (10 km<z< 35 km). The surviving channel can benefit immediately from the excess pump power available due to the decrease in input signal power and a new steady-state distribution of both the pump and the surviving

channel power is established through the Raman fiber. Figure 4.5 shows the distribution of the excess pump power $\Delta P_P(z,t)$, ($\Delta P_p(z,t) = P_p(z,t) - P_p(z,t_0)$, an increase in pump power with respect to an instant when all four channels are on) along the Raman fiber at different instances of time after the two channels (1552 and 1553nm) have been dropped at $t_0 = 0\mu s$. The evolution of the increase in surviving channel power $\Delta P_{sur}(z,t)(\Delta P_{sur}(z,t) = P_{sur}(z,t) - P_{sur}(z,t_0))$ along the fiber is shown (Figure 4.6) for signal wavelength $\lambda_s = 1550\,\text{nm}$.

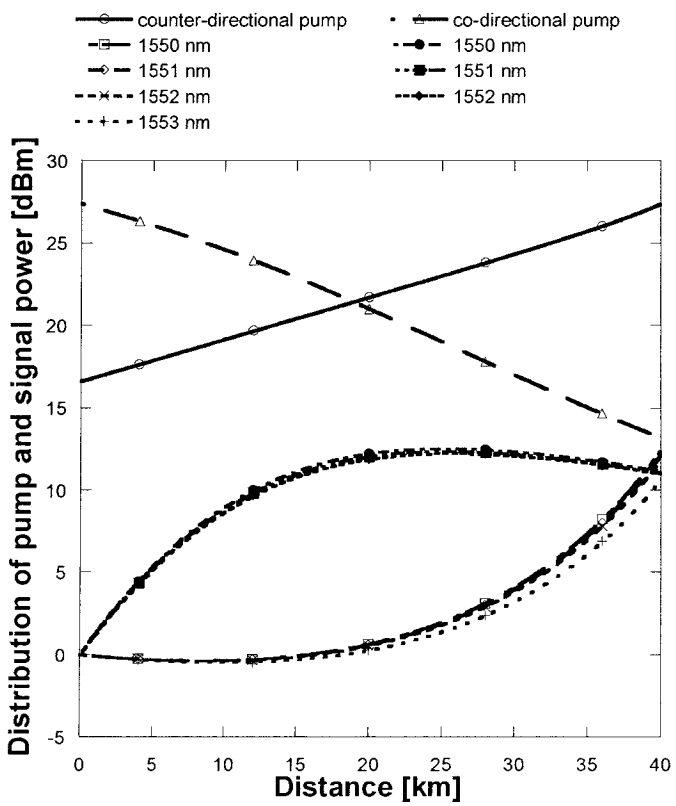

Figure 4.4 Distribution of pump and signal powers along Raman fiber

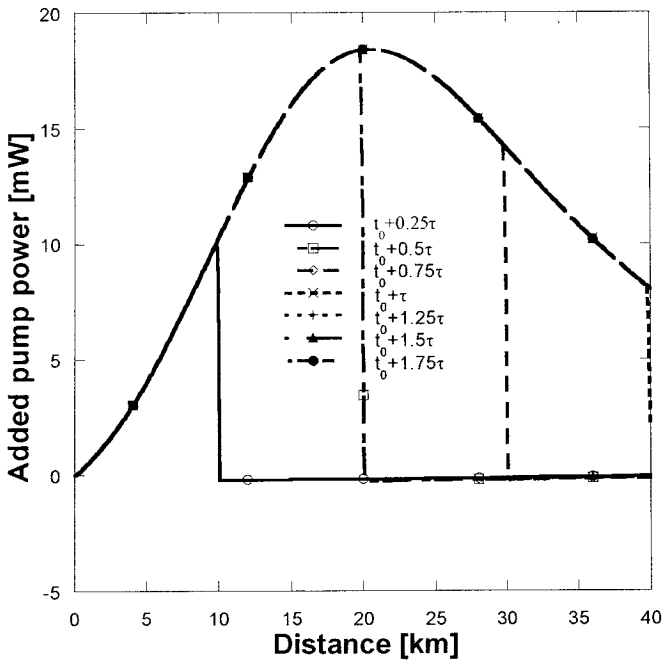

Figure 4.5 Distribution of excess pump power along co-directionally pumped Raman fiber at different instances of time.

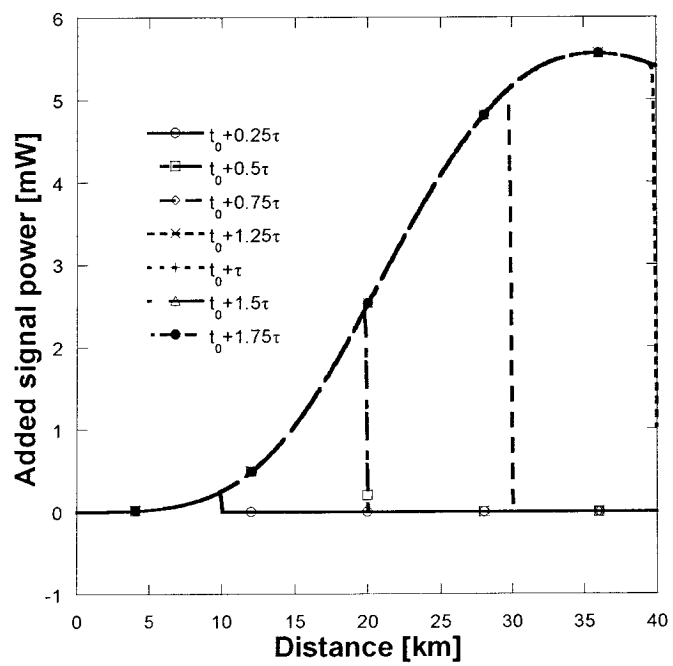

Figure 4.6 Distribution of surviving channel (1550 nm) power fluctuation along co-directionally pumped Raman fiber at different instances of time.

Because counter-directionally pumped FRA signal and pump waves propagate in opposite directions, much longer time is necessary for the new steady-state pump and surviving channel power distributions to settle down when channels are dropped/added. Distribution of excess pump power $\Delta P_p(z,t)$ and the increase in surviving channel power $\Delta P_{sur}(z,t)$ for counter-directionally pumped FRA are shown in Figure 4.7, and 4.8, for several instances of time. In the time interval $t_0 < t < t_0 + \tau$, the front of the surviving channel wave propagates through the region of Raman fiber with the previous steady-state pump power distribution corresponding to all four channels being on, and the surviving channel does not experience any additional gain in this time interval. At $\tau < t < t_0 + 1.5 \bullet \tau$, pump power grows mainly in the region of highest pump depletion (20 km<z< 35 km), and then $t > 1.5 \bullet \tau$, it falls down slightly as the surviving channel power growth cannot be supported by the available pump power. New steady-state pump and surviving channel power distributions settle down at approximately $t = t_0 + 3 \bullet \tau$.

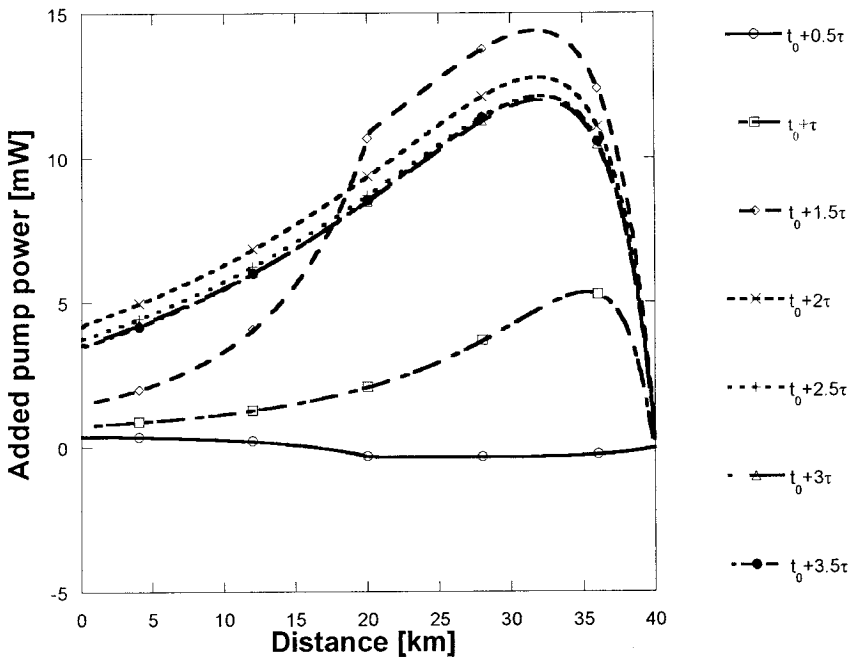

Figure 4.7 Distribution of excess pump power along counter-directionally pumped Raman fiber at different instances of time.

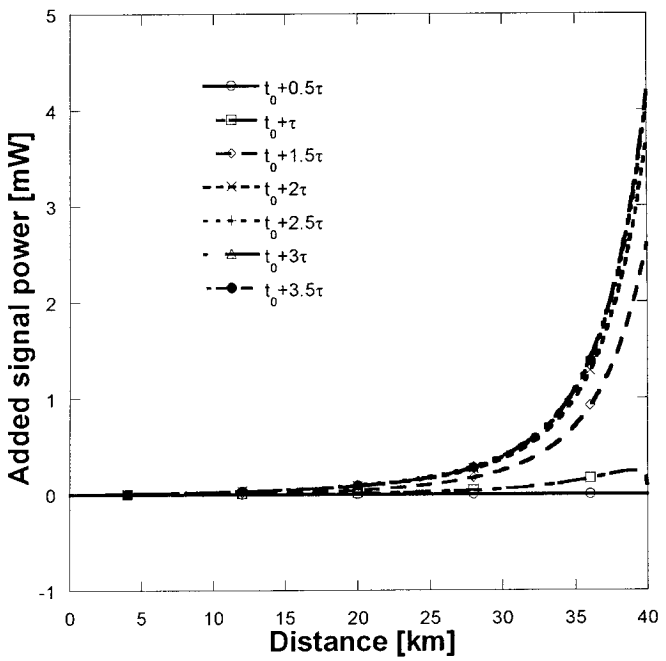

Figure 4.8 Distribution of surviving channel (1550 nm) power fluctuation along Counter-directionally pumped Raman fiber at different instances of time.

It is apparent from the performed analysis that surviving channel power transients in fiber Raman amplifier with co-propagating pumping scheme are so fast and the steady-state condition is soon reached. The power excursion in the co-pumped fiber Raman amplifier is larger than in the counter-pumped case. This may be the fact that the surviving channel in the co-pumped fiber Raman amplifier obtains more pump power than the surviving channel in the counter-pumped fiber Raman amplifier does. In the following analysis we will, therefore, concentrate on the counter-propagating pumping configuration.

4.2.2 Effect of input signal power

The steady-state surviving channel power excursion depends on the input power of WDM channels. It follows from our simulation that the power dynamics is also affected by the input signal power. Figure 4.9 displays surviving channel power variation as a function of time at the output of fiber Raman amplifier (L_{TW_Reach} =40 km; λ_p=1450 nm; P_P^-=550mW; λ_S=1550, 1551, 1552, 1553 nm) for input signal power 0.5, 1, 1.5, 2, and 2.5 mW/channel. With increasing saturation of the fiber Raman amplifier, the steady-state surviving channel excursion increases and the dynamics of the power transients becomes faster. Steady-state power excursion and rise time are 1.789 mW, 4.152 mW, 6.315 mW, 8.252 mW, and 9.993 mW, 221.9 μs , 203.6 μs , 191 μs , 181.3 μs and 173.4 μs for 0.5, 1, 1.5, 2, 2.5 mW/channel, when surviving channel signal wavelength is 1550 nm. To analyze the effect of the number of dropped/added channels on surviving channel dynamics, we simulated the case of counter-directionally pumped fiber Raman amplifier (L_{TW_Reach} =40 km; λ_p =1450 nm; P_P^- =550mW; λ_S =1550, 1551, 1552 and 1553 nm; and 0 dBm/channel) when λ_S =1552; and 1553 nm are dropped and added out

of λ_S =1550, 1551, 1552, and 1553 nm. The power fluctuation of the surviving channel at 1550 nm is plotted in Figure 4.9. The steady-state power excursion is lower (4.18 mW) and the rise time faster (19.6 μs) compared with the case of removal/addition of three out of four signal channels with the same input power (6.71 mW, 203.6 μs , shown in Figure 4.9). At low input levels, transients were barely seen.

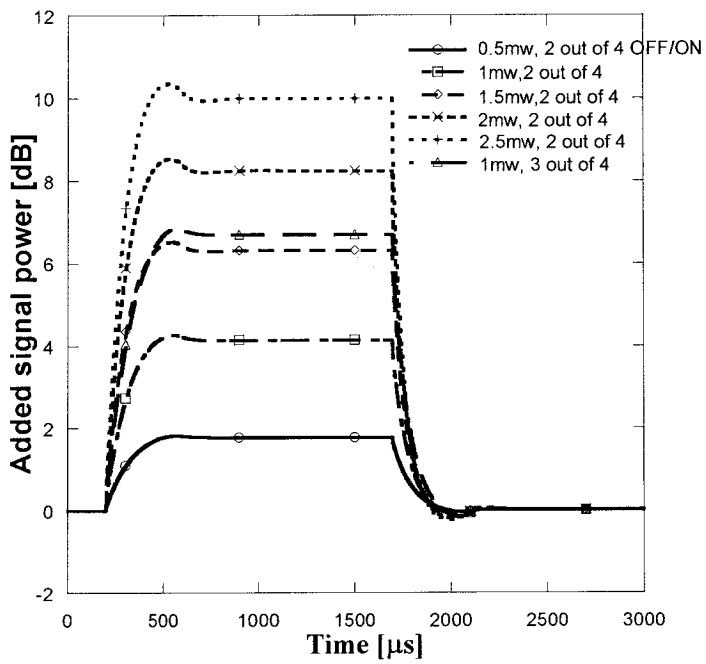

Figure 4.9 Surviving channel (1550 nm) power fluctuation as a function of time.

4.2.3 Effect of Raman fiber length

In the next simulations, pump and input signal power were fixed at P_P^- =550 mW and $P_{s,in}$ =1 mW, respectively, and the effect of Raman fiber length has been studied. Calculated results are summarized in Figure 4.10, where the surviving channel power fluctuation is plotted as a function of time for 20, 40, 60, 80 and 100 km. Steady-state power excursion and rise time were 0.6591, 0.9357, 0.7698, 0.4964, 0.2561 dB and 125.1, 199.6, 257.1, 308.2 and 338 μs for 20, 40, 60, 80 and 100 km, respectively, when

surviving channel wavelength is 1550 nm. At 20 km, the TW Reach fiber is too short so that the available pump power is not fully utilized; more than 145 mW of pump is not absorbed at the end of the TW Reach fiber. On the contrary, for 40, 60, 80 and 100 km, the pump power in the first half of the TW Reach fiber is too low to provide sufficient amplification so that the signal is first attenuated due to internal fiber loss and amplified in the second half of the amplifier. Spatial distribution of pump power and the signal channel power at 1550 nm along the TW Reach fiber are plotted in Figure 4.11, 4.12 for the case that all four signals are amplified. As has already been explained in Section 4.2.1, the surviving channel dynamics in counter-directionally pumped fiber Raman amplifiers depends on the time necessary for the pump power distribution to settle down after channels are dropped/added (Figure 4.7) and, therefore, on the length of the Raman fiber. We have found that the rise time of surviving channel power transients is related to the length of Raman fiber. This relation is, however, nonlinear. The ratio between the rise time and the propagation delay is 1.3027, 1.0342, 0.8866, 0.7964, and 0.6983 for Raman fiber length of 20, 40, 60, 80 and 100 km, respectively, when surviving channel signal wavelength is $\lambda_s = 1550$ nm.

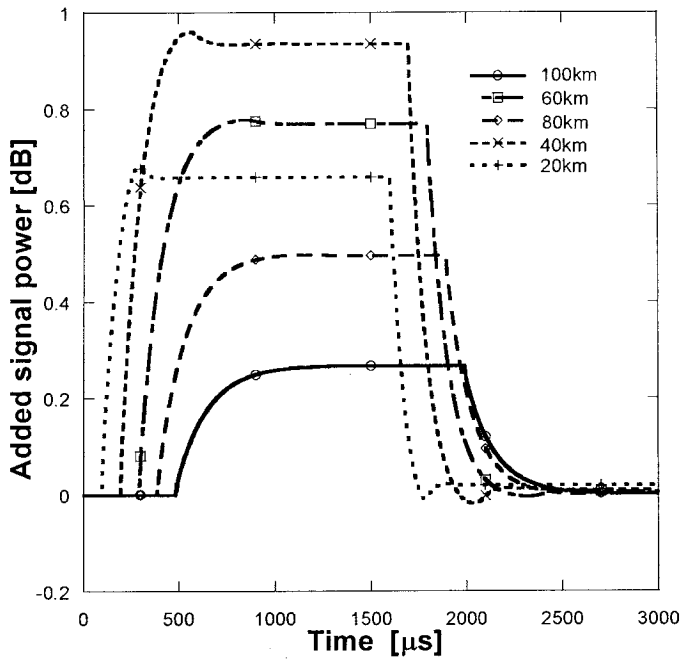

Figure 4.10 Surviving channel (λ_s =1550 nm) power fluctuation as a function of time.

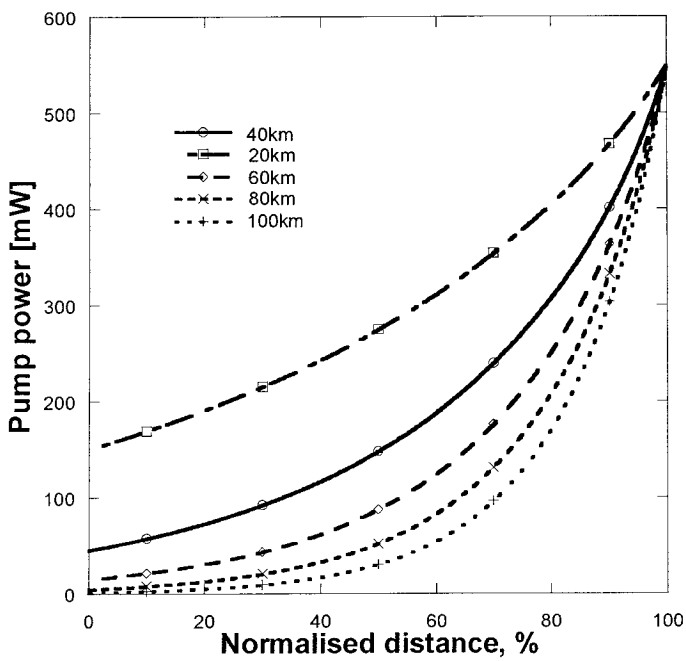

Figure 4.11 Distribution of pump power along Raman fiber: L=20, 40, 60, 80, 100 km.

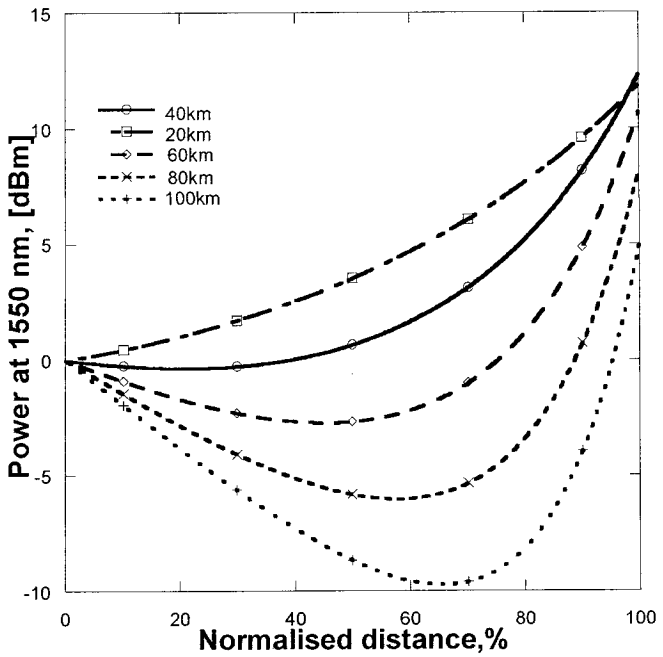

Figure 4.12 Distribution of signal power at λ_s =1550 nm along Raman fiber: L=20, 40, 60, 80, 100 km.

4.2.4 Effect of pump power

The effect of pump power on the dynamics of surviving channel power fluctuations has been investigated for a Raman fiber of length 40 km and input signal power 0 dBm/channel. Figure 4.13 shows surviving channel power fluctuations as a function of time for 400, 450, 500, 550, 600 mW. No leading edge overshoots or undershoots occur when the FRA is pumped by 400 mW. Steady-state surviving channel power excursion and rise time are 0.4413, 0.5896, 0.7559, 0.9298 and 1.1 dB and 223.4, 217.3, 208.9, 198.4, and 185.7 μs for 400, 450 500,550, and 600 mW, respectively, when surviving channel signal is λ_s =1550 nm.

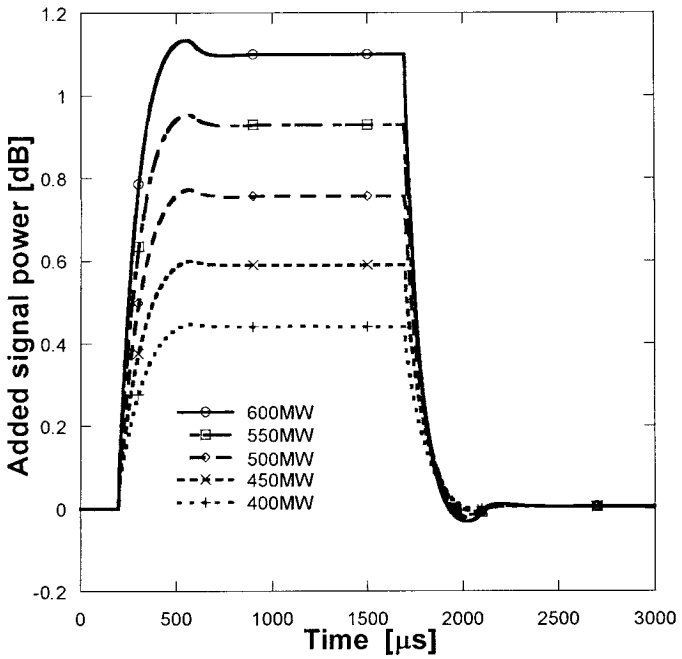

Figure 4.13 Surviving channel (λ_s =1550 nm) power fluctuation as a function of time.

4.2.5 Effect of transients as a function of fiber type

Fiber type can affect pump-depletion level and cause very different transient behaviors. For the two fiber types under study, standard silica fiber (SMF28) and TW Reach fiber, SMF28 has a small Raman gain coefficient and a slightly larger group velocity mismatch between pump and signal. Both characteristics of SMF28 contribute to less pump depletion through smaller peak signal level and larger pump-signal walkoff, consequently, SMF28-based Raman will exhibit weaker transients for the same input signal levels and pump powers. Figure 4.14 plots the power transient comparison between SMF28 and TW Reach fiber for a surviving channel for input signal power 1mW/channel. In the counter-pumping configuration, much weaker transients were observed in SMF28 fiber in comparison to TW Reach fiber under the same pumping conditions. Steady-state surviving channel power excursion and rise time are 0.93, 0.183

dB and 233, 244 μs for TW Reach fiber and SMF28 fiber, respectively, when surviving channel signal wavelength is $\lambda_s = 1550$ nm.

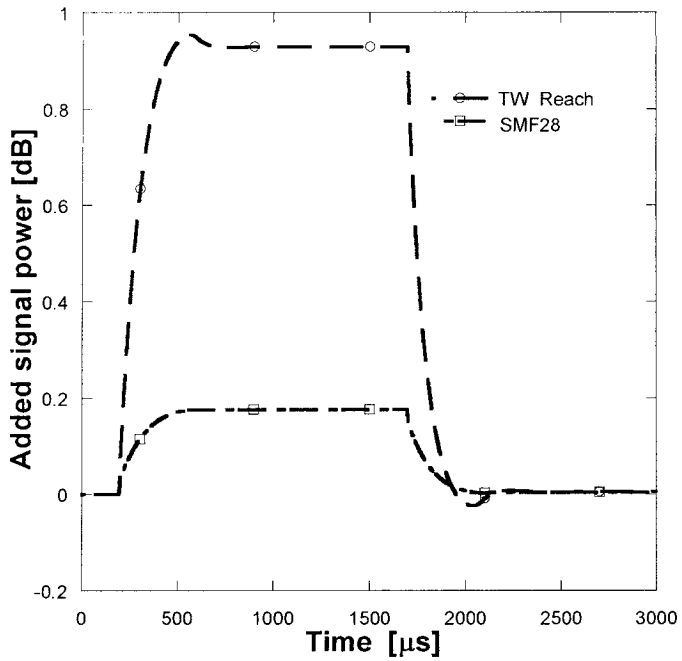

Figure 4.14 Comparison of transient behavior between TWRS and SMF28 fibers for surviving channel 1550 nm (counter-pumping, input power 1 mw)

4.3 Effect of transients as a function of surviving signal wavelength

When only one different wavelength signal is dropped/added, we may monitor the surviving signal power transient. We assume that 40 km of TW Reach fiber is pumped counter-directionally by 550 mw, and the input signal power is 1mW/channel. The wavelengths of signal are λ_s=1550, 1520, 1556 nm, respectively. The signal channel λ_s=1550 nm exhibits the strongest transient, because the signal λ_s=1550 nm gets more energy from pump. The signal λ_s=1520 nm get least energy from pump, because of smaller Raman gain coefficient. The large overshoot at the leading edge of the signal (λ_s=1550, 1556 nm) is caused by the unsaturated gain that the signal experiences. The

strong power of the signal (1550 nm) front depletes the pump. As a result, the remaining signal pulse does not experience the same high gain as the leading edge of the signal. Pump depletion is strongest when the signal front reaches the output of the fiber. The depleted pump propagates backward in the TW Reach fiber and produces a gain that is smaller than the steady-state saturated gain. This causes the small undershoot in the signal power in figure 4.15. After one complete round-trip delay, signal and pump power fluctuations within the amplifier diminish, which lead to reduced fluctuations at the output of the Raman amplifier after an additional propagation delay.

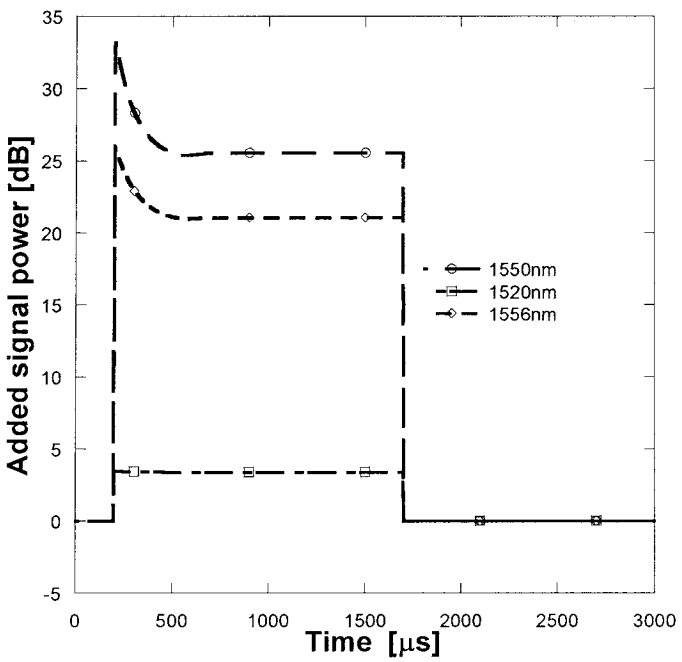

Figure 4.15 Surviving channel (λ_s =1550 nm, 1520 nm, 1556 nm) power fluctuation as a function of time along Raman fiber: L=40 km; λ_p =1450 nm; P_p =550 mW; $P_{s,in}$ =1 mW/channel;

4.4 Effect of the number of dropped/added channels

The power transients are analyzed in Raman amplifiers considering three pump configurations and added-dropped different the number of signal channels in a 6

channels-WDM system using TW Reach fiber as Raman gain media. The fiber length for the fiber Raman amplifiers is 40 km. The pump in fiber Raman amplifiers was fixed at λ_p=1450 nm and its total power was 550mW for TW Reach fiber, for the counter-pumped, co-pumped and bi-directional pumped schemes. In the bi-directional pump scheme the power is split at half for each pump laser.

The system stimulated has 6 channels occupying a bandwidth of 6 nm ranging from 1550 nm to 1555 nm and channel spacing equals to 1 nm. Each input signal launches 1mW optical power into the fiber.

Some of the channels in the system are dropped/added. Five different patterns were considered here. In the first one, we dropped and then added 5 signals (1551 nm, 1552 nm, 1553 nm, 1554 nm and 1555 nm). In the second one, the procedure is repeated with 4 signals (1552 nm, 1553 nm, 1554 nm and 1555 nm). In the third one, the procedure is repeated with 3 signals (1553 nm, 1554 nm and 1555 nm). In the fourth one, the procedure is repeated with 2 signals (1554 nm and 1555 nm). Finally, in the fourth one, one signals 1555 nm is added-dropped. The signals are always dropped at $0\ \mu s$ and added at $1000\ \mu s$.

Figure 4.16, 4.17 and 4.18 show the power excursions on a surviving channel at 1550 nm for the fiber Raman amplifiers counter-pumped, co-pumped and bi-pumped when 5, 4, 3, 2 and 1 signal channels are added-dropped.

The leading-edge (drop of channels) in the output signal has overshoots and then reaches a new steady-state condition with approximately 2.57 dB higher than the initial condition for signal 1550 nm. In the trailing-edge, (add of channels) the output signal has undershoots and then the signal reaches the steady-state condition again. The transients in

leading-edge are caused by the lower saturated gain that the surviving channels experience when some channels are dropped. The stronger power in the front signal leads to the depletion of the pump, and the remaining signal does not experience the same gain as in the leading edge due to the lower pump power. In the case of the trailing-edge, after the addition of the channels, the pump is more depleted, and because it propagates backward, the signal gets a lower gain than the steady-state saturated gain.

Unlike the counter-pumped fiber Raman amplifiers, in the co-pumped configuration the overshoot and undershoot were not noticed, as showed in Figure 4.17. Even when the number of added/dropped channels was increased, the presence of them was not clearly noticed. The transients occur faster in the co-pumped fiber Raman amplifiers due to the fact that the pump and surviving signals are propagating in the same direction with approximately the same group-velocities.

Finally, the bi-directional pumping scheme seems to have an intermediate response between the co and counter pumped ones. The overshoot and undershoot are lower than the counter-pumped, but larger than the co-pumped scheme. Regarding the speed of the transients, we noticed the same pattern: they are faster than the counter-pumped, but not as fast as the co-pumped fiber Raman amplifiers.

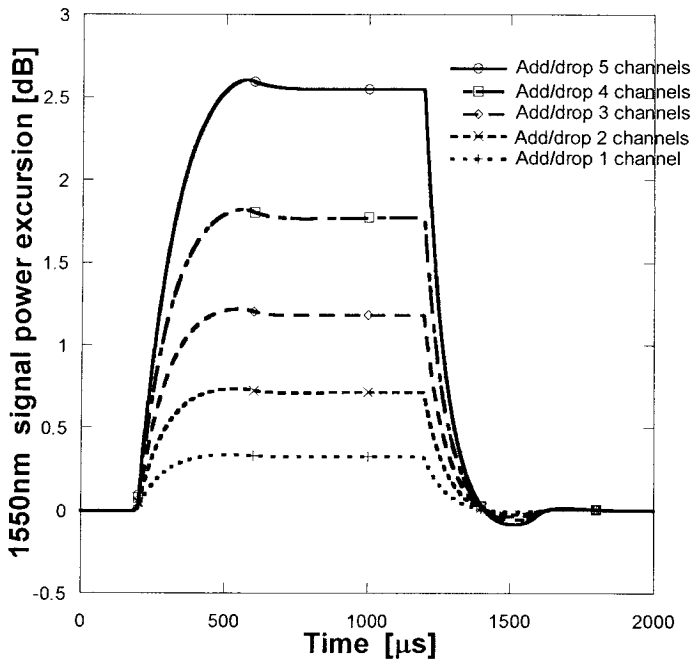

Figure 4.16 Output-surviving signal at λ_s =1550 nm for TW Reach fiber counter-pumped.

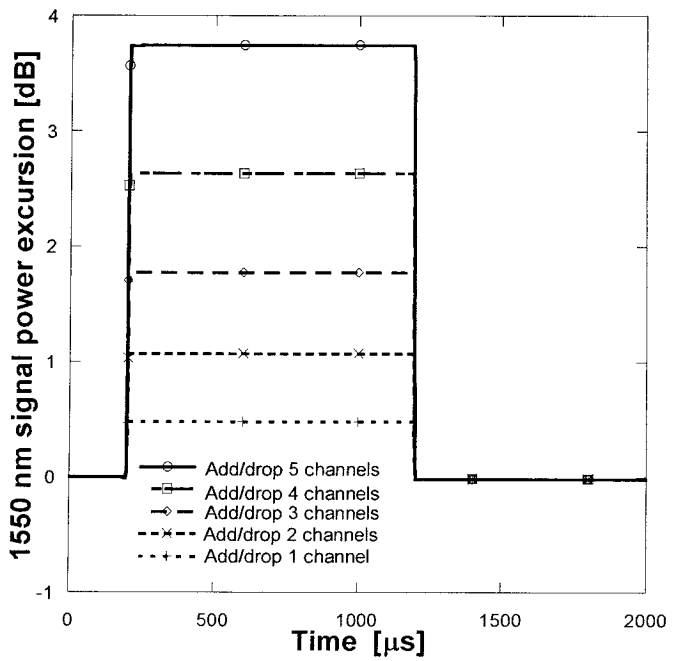

Figure 4.17 Output-surviving signal at λ_s =1550 nm for TW Reach fiber codirectional-pumped.

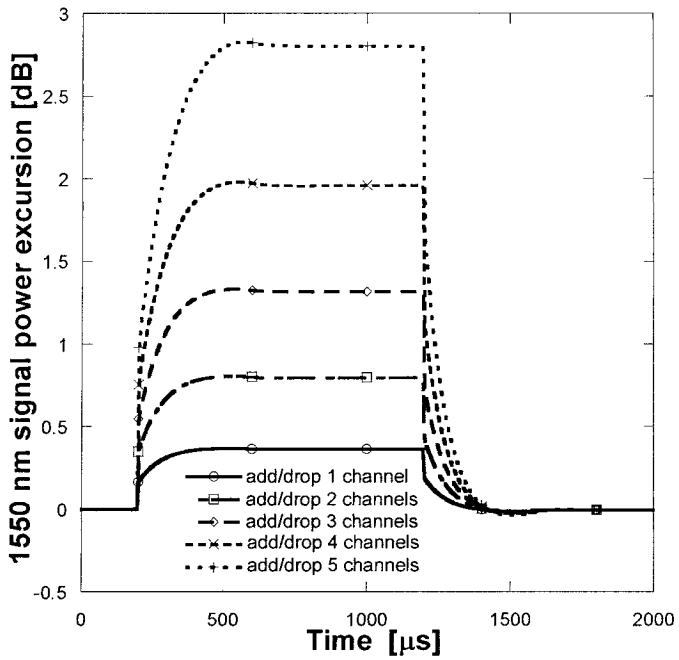

Figure 4.18 Output-surviving signal at λ_s=1550 nm for a TW Reach fiber bidirectional-pumped.

Chapter 5 Transient Analysis of Fiber Raman Amplifiers with Multiple Coherent Pumps

We will analyze surviving channel power change in gain-flattened multipump fiber Raman amplifiers designed for DWDM application and multipump power change along the Raman amplifiers, when some signal channels are dropped/added. In Chapter 5, fiber Raman amplifier steady state analysis with multiple coherent pumps is presented in Section 5.1. Surviving channel power transient effects and multiple pump power change in the fiber Raman amplifier counter-directionally pumped by multiple coherent pumps are presented in Section 5.2. The amplifier with flat gain in C+L band range consists of L=100 km of TW Reach fiber counter-directionally pumped by six counter-pumping sources. The fiber Raman gain medium is TW Reach fiber, which has the following measured parameters: fiber loss changing from 0.4 dB/km at 1262 nm to 0.2 dB/km at 1573 nm with the water peak loss of 0.33 dB/km at 1382 nm, Rayleigh scattering coefficient varying from -33.7 dB/km at 1500 nm to -35.4 dB/km at 1620 nm, effective fiber core area increasing from 46 μm^2 at 1440 nm to 58 μm^2 at 1590 nm, and Raman gain coefficient peaked at 0.608 $(W \cdot km)^{-1}$ with a frequency shift of 13.3 THz measured by pumping at 1460 nm. To get the group velocity, one equation: $V_g(\lambda_2) = 1/(1/V_g(\lambda_1) + \int_{\lambda_1}^{\lambda_2} D(\lambda))$, where $V_g(\lambda_1)$ is the group velocity in the fiber at wavelength λ_1 and $D(\lambda)(D(\lambda) \approx S_0(\lambda - \lambda_0)$, $S_0 = 0.045\ ps/(nm^2 \cdot km)$ - the slope of the

dispersion at the zero-dispersion wavelength of λ_0=1405 nm. The parameters used are: 92 signal channels with channel spacing of 100 GHZ over the spectrum of 1530 to 1605 nm, 1mW per channel for input power. By optimization of the pumping wavelengths to obtain the flattest gain, the optimized wavelengths/powers are 1425nm/160mW, 1434nm/130mW, 1445nm/108mW, 1461nm/75mW, 1482nm/73mW, and 1502nm/60mW. The ASE spectral components are calculated in the wavelength range from 1480 to 1640 nm with resolution of $\Delta\lambda_{ASE}$=1 nm.

5.1 Steady state analysis

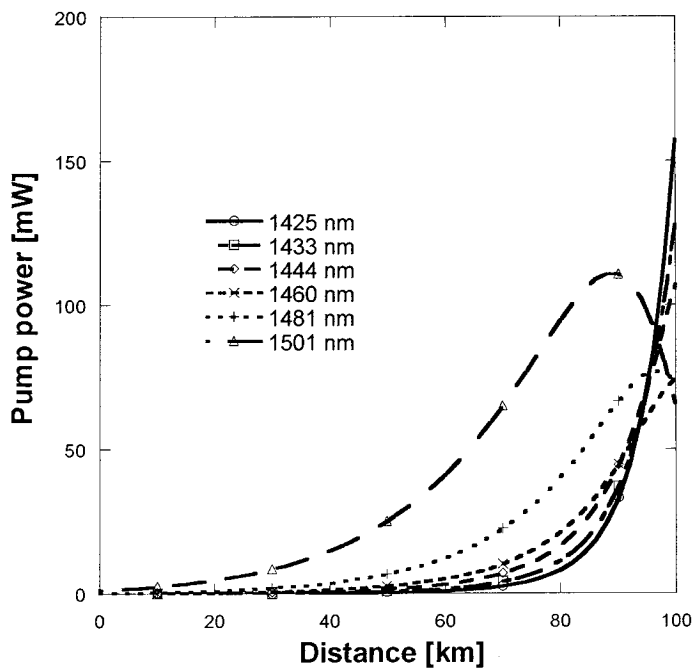

Figure 5.1 Distribution of pump power along Raman fiber for pump 1425, 1433, 1444, 1460, 1481, and 1501 nm.

After the steady-state distribution of forward and backward propagating optical power is calculated, spatial distribution of pump powers is depicted in Figure 5.1. Because of signal-to-signal interactions, shorter-wavelength pumps can amplify longer-wavelength ones, so that the pumps at 1482 and 1502 nm start to rise at the beginning of

their propagation. Optimized pump wavelengths and powers must be carefully designed to obtain flat gain-wavelength characteristic of a multipump FRA. Calculated net gain of FRAs ranges from 9.6 to 10.4 dB for six coherent pumps [39]. Optical spectrum at the output of the FRAs is shown in Figure 5.2.

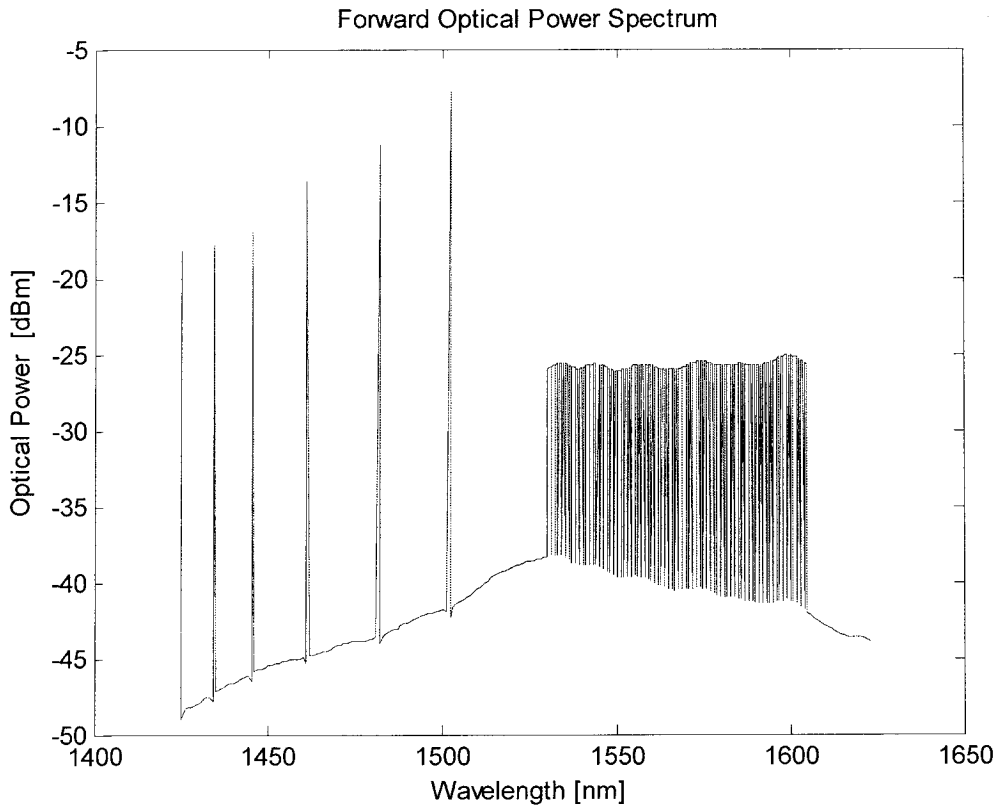

Figure 5.2 Output spectrum of the Raman fiber amplifier.

5.2 Transient analysis

The surviving channel power fluctuations depend on the position of the dropped/added channels within the considered spectrum. Therefore, three different drop/add cases are considered: (a) L band drop/add, (b) C band drop/add, (c) every other channel drop/add. For all three cases, we suppose that dropping/adding channels are dropped at the time t= t_0 =0 μs and added again at the time t=1000 μs . The light

transmission time over 100-km TW Reach fiber is $\tau = 490\ \mu s$. Figure 5.3, 5.4, and 5.5 show some surviving channel power changes for the above three cases with six coherent pumps. When L-band channels are first dropped from the FRAs and then added into the FRAs (case (a)), the surviving channel power changes for some wavelengths of 1530, 1539.43, 1548.97, and 1558.64 nm with six coherent pumps are shown in Figure 5.3. It is seen that the surviving channel power is increased by ~1.2 dB due to dropping the L-band, dependent on the wavelength of the surviving channels. The shortest wavelength (1530 nm) in the surviving channels suffers from the most serious power increase, and the longest wavelength (1558.64 nm) suffers from the lowest power burst. This is due to the fact that longer-wavelength channels are amplified by the shorter-wavelength ones and the shorter wavelength signal channels experience stronger pump depletion than the longer wavelength signal channels do. Because of signal-to-signal Raman interactions, when the L-band is added, the shorter wavelengths have faster response than the longer wavelengths. For the case (b) shown in Figure 5.4, when the C-band is dropped, the L-band channels have a decrease in power (undershoot). This is because the C-band channels act as pumps for the L-band when the C-band channels are suddenly dropped to cause a decrease in gain due to the loss of signal-to-signal amplification. The L-band signals power gradually increase to a certain level, dependent on wavelengths. Because surviving signal channel power transient is governed by the pump power change seen by the signals and shorter wavelength surviving signal channels experience relative much stronger pump depletion than longer wavelength surviving signal channels do, the power level for shorter wavelengths is higher than longer wavelengths as shown in Figure 5.4. When the C-band is added back, the surviving channels suffer from an over-shoot in

power. This is due to signal-to-signal interaction. Longer wavelength signals are amplified by the shorter wavelength ones. For the case (c) as shown in Figure 5.5, when every other channel is dropped and added, the surviving channels suffer from power undershoots for the longer wavelength surviving channels because the loss in gain caused by the drop of shorter wavelength channels. When the dropped channels are added, overshoots for the longer wavelength surviving channels result from signal-to-signal interactions. By carefully observing three figures in Figure 5.3, 5.4 and 5.5, we can find that FRAs have quite different transient behaviors. The surviving channel signal power due to transient is 1.2, 0.6 and 1 dB for the three cases with six coherent pumps in Figure 5.3, 5.4, and 5.5.

Because power transients in Raman amplification are determined by pump power change compared with the previous steady-state pump power distribution corresponding to all channels being on. We analyzed the multipump power change to know different wavelength pumps having different power change. Because input signal power is decreased, the surviving signals will experience stronger pump depletion and establish a new steady-state distribution of the pump power behind the front of the surviving channel wave as it propagates through the Raman fiber. Because of signal and pump waves propagate in opposite directions, long rise and fall times of surviving channel power transients in counter-directionally pumped FRAs are caused and much longer time is necessary for the new steady-state pump power distribution to settle down when channels are dropped/added.

We calculate the pump power change due to the transient by $\Delta P_p(z,t) = P_p(z,t) - P_p(z,t_0)$, where $P_p(z,t)$ is the pump power at a distance z and time

t when transient occurs, and $P_p(z,t_0)$ is the pump power at the steady state. Thus a positive $\Delta P_p(z,t)$ means excess pump power available for surviving signal channels and a negative $\Delta P_p(z,t)$ means less pump power available for surviving signal channels. Corresponding to Figure 5.3, 5.4, 5.5, L-band (case (a)), or C-band (case (b)) or every other channel (case (c)) is dropped respectively. Figure 5.6, 5.7, and 5.8, each shows six pump powers change along the distance at the times of $t_0 + 0.5\tau$ =245 μs, $t_0 + \tau$ = 490 μs, $t_0 + 1.5\tau = 735$ μs, and $t_0 + 2\tau = 980$ μs. For the cases (a), (b) and (c) as shown in Figure 5.3, 5.4, and 5.5, the change of pump power for all six pumps is most significant due to transient in the position of 70-90 km (input signals at the position of 0 km). We have found that when the time is beyond $t_0 + 2\tau$, the pump power is hardly changed with time. This suggests that a new steady-state pump power distribution is established. Moreover, it is shown that the new steady-state pump power distribution is different from the previous steady-state pump power distribution with all channels on. The steady-state pump power distribution increases due to transient in longer wavelength pumps, while it decreases in shorter wavelength pumps. For example, in the case (a) the steady-state pump power increases by ~7 mW at 1502 nm, by ~1 mW at 1461nm, by ~4 mW at 1482nm; it decreases by ~3 mW at 1425 nm, by ~1.3 mW at 1434 nm, by ~1.3 mW at 1445 nm. In the case (b) the steady-state pump power increases by ~1 mW at 1445 nm, by ~1.7 mW at 1461 nm, by ~2.5 mW at 1482 nm and by ~4.5 mW at 1502 nm; it decreases ~2.5 mW at 1425 nm, by ~1.5 mW at 1434 nm. In the case (c) the steady-state pump power increases by ~0.6 mW at 1445 nm, by ~1.3 mW at 1461 nm, by ~3.2 mW at 1482 nm, by ~5.5 mW at 1502 nm; it decreases by ~2.5 mW at 1425 nm, by ~1.5 mW at

1434 nm, by ~0.8 pump power at 1445nm. Among the three cases, the excess pump powers at longer wavelength 1482 and 1502 nm in case (a), as shown Figure 5.6, is the highest; while the excess pump powers at 1482 and 1502 nm in case (b), as shown Figure 5.7, is the lowest and the excess pump powers at 1482 and 1502 nm in case (c), as shown Figure 5.8, lie between case (a) and case (b). In the three cases, the pump powers increased at 1482 and 1502 nm are higher than that at other wavelength, since longer-wavelength pumps could be amplified by the shorter-wavelength ones due to signal-to-signal interactions.

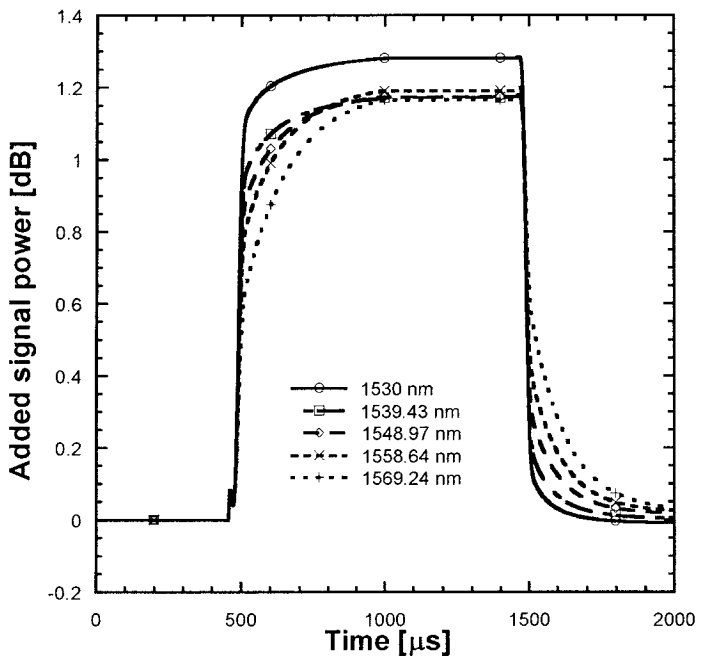

Figure 5.3 Surviving channel power fluctuation as a function of time when the L band out of L+C band channels are dropped/added.

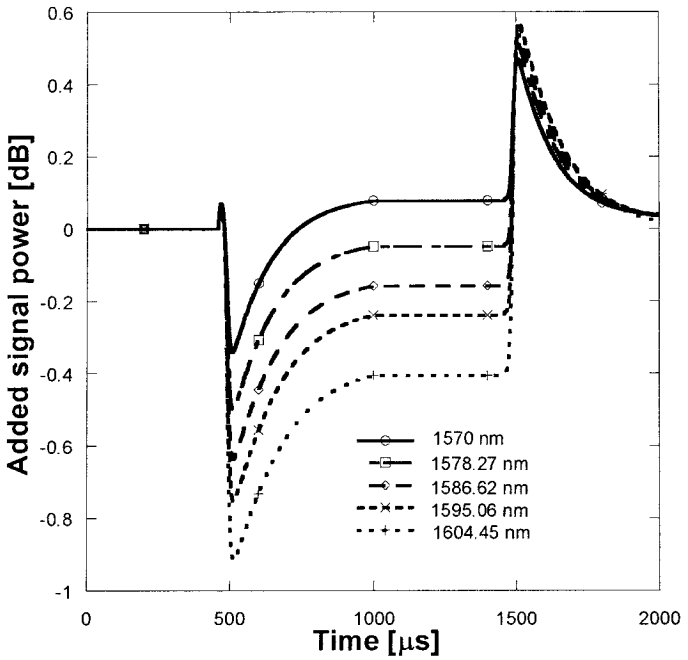

Figure 5.4 Surviving channel power fluctuation as a function of time when the C band out of L+C band channels are dropped/added.

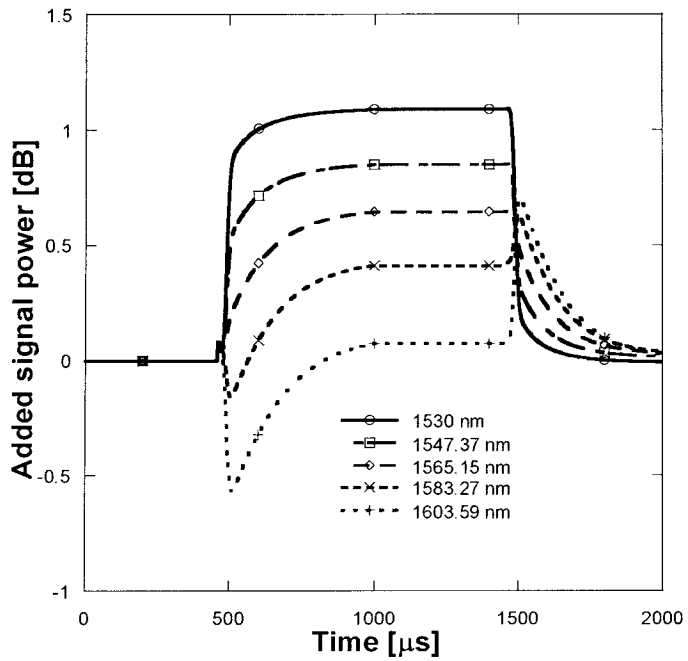

Figure 5.5 Surviving channel power fluctuation as a function of time when every other channel is dropped/added.

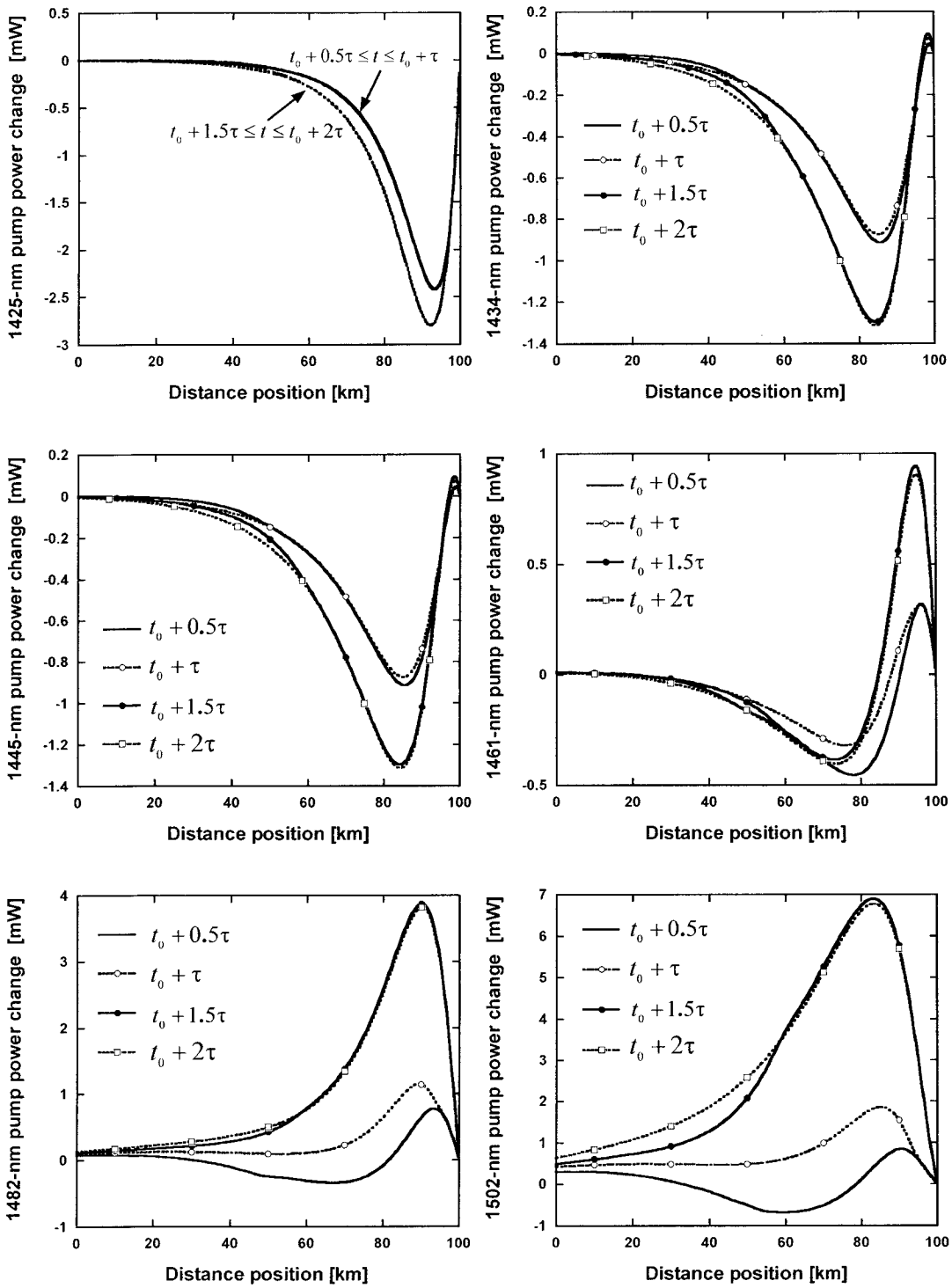

Figure 5.6 Distribution of pump power change related to the steady state along the fiber due to transient at the time: $t_0+0.5\tau$, $t_0+\tau$, $t_0+1.5\tau$ and $t_0+2\tau$. L-band channels are dropped.

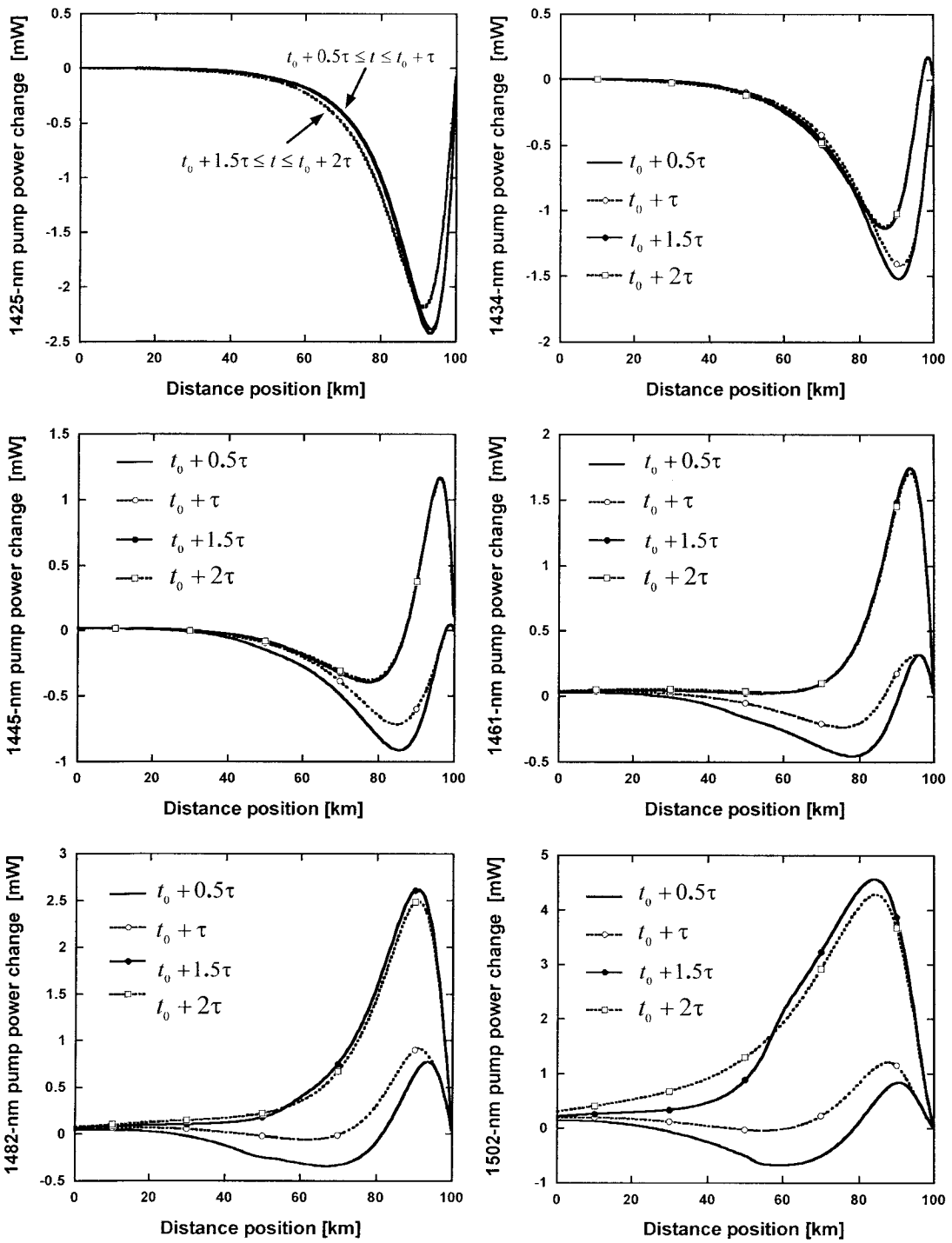

Figure 5.7 Distribution of pump power change related to the steady state along the fiber due to transient at the time: $t_0+0.5\tau$, $t_0+\tau$, $t_0+1.5\tau$ and $t_0+2\tau$. C-band channels are dropped.

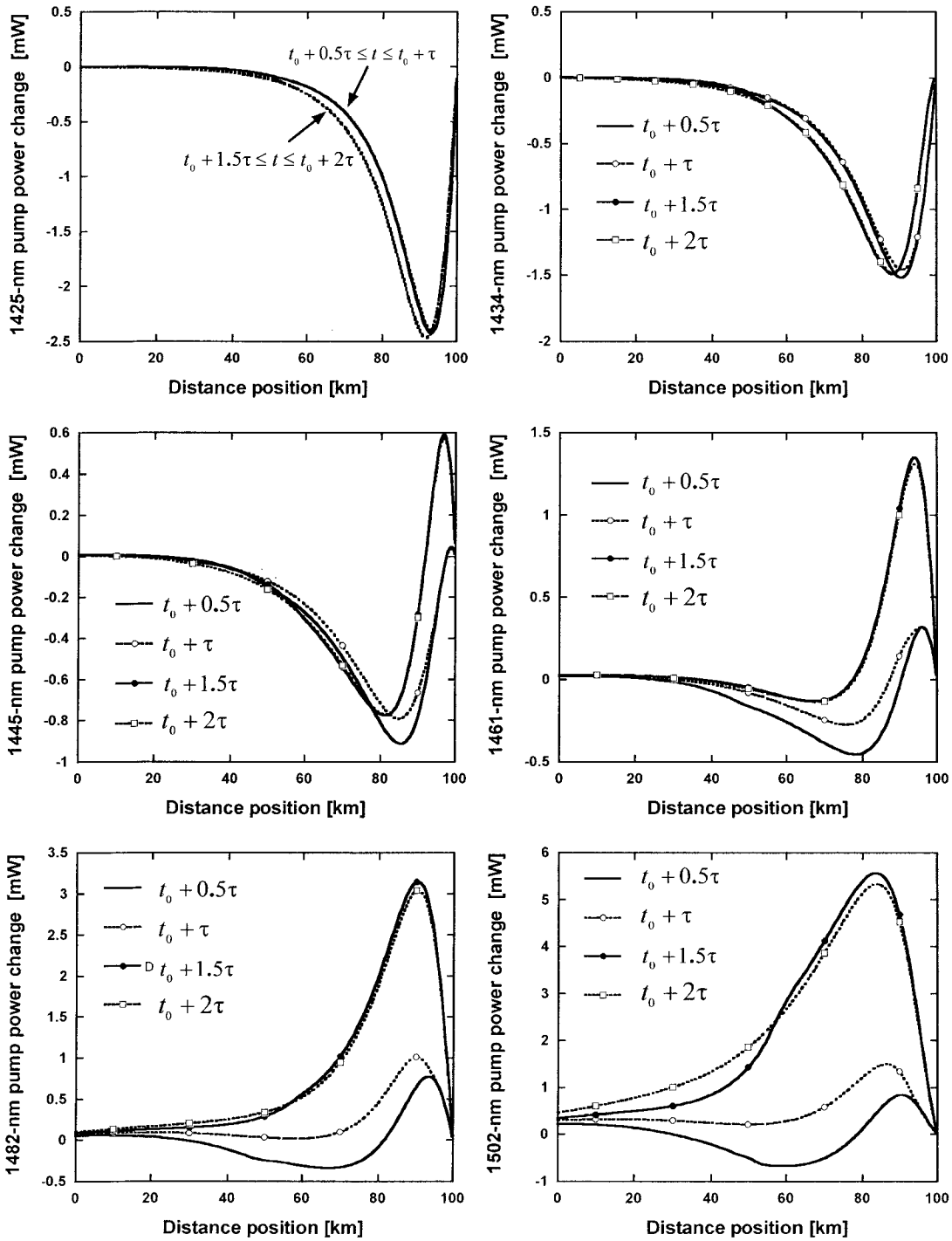

Figure 5.8 Distribution of pump power change related to the steady state along the fiber due to transient at the time: $t_0+0.5\tau$, $t_0+\tau$, $t_0+1.5\tau$ and $t_0+2\tau$. every other channel is dropped.

Chapter 6 Transient Analysis of Fiber Raman Amplifiers with Multiple Incoherent Pumps

In Chapter 6, fiber Raman amplifier characteristics with multiple incoherent pumps are presented in Section 6.1. Fiber Raman amplifier steady state analysis with multiple incoherent pumps is presented in Section 6.2. Surviving channel power transient effects and incoherent pump power changes in FRAs counter-directionally pumped by incoherent pumping are presented in Section 6.3. Comparison of power transients in fiber Raman amplifiers with multiple coherent pumping or incoherent pumping is presented in Section 6.4. The fiber Raman gain medium is TW Reach fiber, which has the following measured parameters: fiber loss changing from 0.4 dB/km at 1262 nm to 0.2 dB/km at 1573 nm with the water peak loss of 0.33 dB/km at 1382 nm, Rayleigh scattering coefficient varying from -33.7 dB/km at 1500 nm to -35.4 dB/km at 1620 nm, effective fiber core area increasing from 46 μm^2 at 1440 nm to 58 μm^2 at 1590 nm, and Raman gain coefficient peaked at 0.608 $(W \cdot km)^{-1}$ with a frequency shift of 13.3 THz measured by pumping at 1460 nm. To get the group velocity, one equation: $V_g(\lambda_2) = 1/(1/V_g(\lambda_1) + \int_{\lambda_1}^{\lambda_2} D(\lambda))$, where $V_g(\lambda_1)$ is the group velocity in the fiber at wavelength λ_1 and $D(\lambda)(D(\lambda) \approx S_0(\lambda - \lambda_0)$, S_0= 0.045 $ps/(nm^2 \cdot km)$- the slope of the dispersion at the zero-dispersion wavelength of λ_0=1405 nm. The parameters used are:

92 signal channels with channel spacing of 100 GHZ over the spectrum of 1530 to 1605 nm (C+L bands), 1 mW input power per channel.

6.1 Raman amplifier characteristics with incoherent pumping

In contrast to the conventional coherent pumping source, the pumping power of incoherent pumping source spreads over a wide wavelength range from several nanometers to tens of nanometers, and the phase and polarization of incoherent pumping source are completely random. Thus, the SBS impairment can be completely suppressed by using incoherent pumping due to its wide spectral width. Due to the random phase of incoherent pumps, the FWM generation by the interaction of pump-pump, pump-ASE noise and pump-signal can be significantly reduced. Another advantage of using incoherent pumping is that the polarization multiplexer for pumping sources may be eliminated due to the random polarization of pumping sources. For FRAs with incoherent pumping, the signal amplification by Raman gain is given by the summation effect from pump power in the whole pump spectral bandwidth.

6.2 Steady state analysis

After the steady-state distribution of forward and backward propagating optical power is calculated, we can get spatial distribution of pump powers, signal powers and ASEs powers. By optimization of the two incoherent pumping wavelengths to obtain the flattest gain, it is found that the incoherent pumping sources should have a wavelength at 1429 nm (571 mW) with a FWHM of 20 nm, and the other wavelength at 1491 nm (96 mW) with a FWHM of 20 nm. The resulting on-off Raman gain is ~10 dB with a ripple of ~1 dB over 1530 – 1605 nm by two incoherent pumps [39]. Optical spectrum at the output of the FRAs is shown in Figure 6.1.

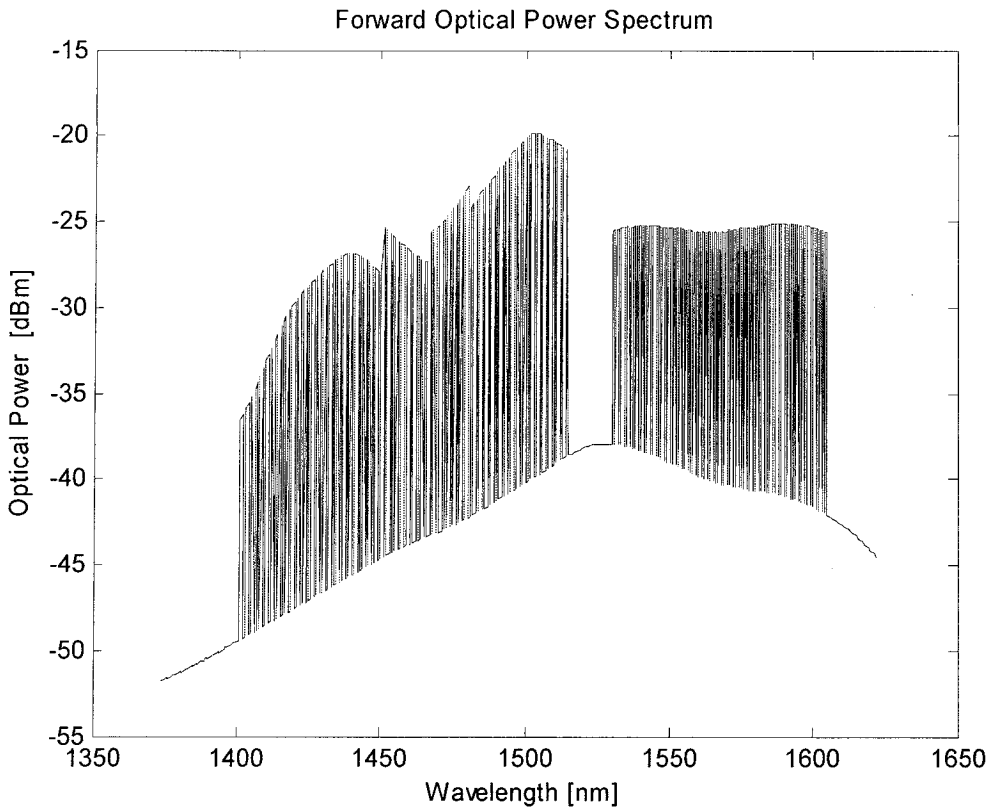

Figure 6.1 Output spectrum of the Raman fiber amplifier.

6.3 The surviving signal channel power transient analysis

The amplifier consists of 100 km of TW Reach counter-directionally pumped by two incoherent pumping sources. Next we analyze surviving channel power change in distributed FRAs with two incoherent pumps when some signal channels are dropped/added. The FRA consists of fiber length of TW-Reach 100 km, counter-pumped by with two incoherent pumps. The surviving channel power fluctuation depends on the position of the dropped/added channels within the considered spectrum. Therefore, three different drop/add cases are considered: (a) L band drop/add, (b) C band drop/add, (c) every other channel drop/add. For all three cases, we suppose that dropping/adding

channels are dropped at the time t=t_0=0 μs and added again at the time t=1000 μs. The light transmission time over 100-km TW Reach fiber is $\tau = 490$ μs. Figure 6.2, 6.3 and 6.4 show some surviving channel power change for the above three cases with two incoherent pumps. When L-band channels are first dropped from the FRA and then added into the FRA (case (a)), the surviving channel power changes for some wavelengths of 1530, 1539.43, 1548.97, and 1558.64 nm with two incoherent pumps are shown in Figure 6.2. It is seen that the surviving channel power is increased by ~1.2 dB due to dropping the L-band, dependent on the wavelength of the surviving channels. The shortest wavelength (1530 nm) in the surviving channels suffers from the most serious power increase, and the longest wavelength (1558.64) suffers from the lowest power burst. This is due to the fact that the shorter wavelengths experience relative much larger pump power change relative to longer wavelength surviving signal channels. Because of signal-to-signal Raman interactions, when the L-band is added, the shorter wavelengths have faster response than the longer wavelengths. For the case (b) shown in Figure 6.3, when the C-band is dropped, the surviving L-band channels have a decrease in power (undershoot). This is because the C-band channels act as pumps for the L-band when C-band channels are suddenly dropped to cause a decrease in gain due to the loss of signal-to-signal amplification. The L-band signal power gradually increases to a certain level, dependent on wavelengths. Because surviving signal channel power transients are governed by the pump power change seen by the signals and shorter wavelength surviving signal channels experience relative much stronger pump depletion than longer wavelength surviving signal channels do, the power level for shorter wavelengths is higher than longer wavelengths as shown in Figure 6.4. When the C-band is added back,

the surviving channels suffer from an over-shoot in power. This is due to signal-to-signal interaction. Longer wavelength signals are amplified by the shorter wavelength ones. For the case (c) as shown in Figure 6.4, when every other channel is dropped and added, the surviving channels suffer from power undershoots for the longer wavelengths surviving channels because the loss in gain caused by the drop of shorter wavelength channels. When the dropped channels are added, overshoots for the longer wavelength surviving channels result from signal-to-signal interactions. The surviving signal power due to transient is 1.2, 0.6 and 1 dB respectively for the three cases with two incoherent pumps in Figures 6.2, 6.3, and 6.4.

Power transients in Raman amplification are determined by pump power change that new steady-state pump power distribution is compared with the previous steady-state pump power distribution corresponding to all channels being on. The incoherent pump power change is analyzed. When input signal power is decreased, the surviving signals get more incoherent pump power and establish a new steady-state distribution of the pump power. We calculated the distribution of incoherent pump power change $\Delta P_p(z,t)$ along the Raman fiber at several different positions and at different instances of time after the L band, the C band, and every other channel signal, have been dropped respectively at t_0=0 μs. Because signal and pump waves propagate in opposite directions, long rise and fall times of surviving channel power transients in counter-directionally pumped FRAs occur and much longer time is necessary for the new steady-state pump power distribution to settle down when signal channels are dropped/added.

Figure 6.5, Figure 6.6 and Figure 6.7 show distributions of incoherent pump power change $\Delta P_p(z,t)$ for counter-directionally pumped FRAs at several different positions

along the Raman fiber and several instances of time in case (a), case (b) and case (c) respectively. In case (a), (b), or (c) incoherent pump power changes are different. The new established area of shorter wavelength pump power compared with previous steady-state pump with the same pump wavelength power distribution area corresponding to all channels being on decreases due to energy transfer from shorter wavelength pump to longer wavelength pump. For the same reason, the new established area of longer wavelength pump power compared with previous steady-state pump with the same pump wavelength power distribution corresponding to all channels being on increases. Among case (a), (b), and (c), power changes in the longer wavelength pump area are different. The power change in case (a) is the highest, while the power change in case (b) is the lowest and the power change in case (c) lies between that in case (a) and case (b). A new steady-state pump power distribution settles down at approximately $t = t_0 + 2 \bullet \tau$.

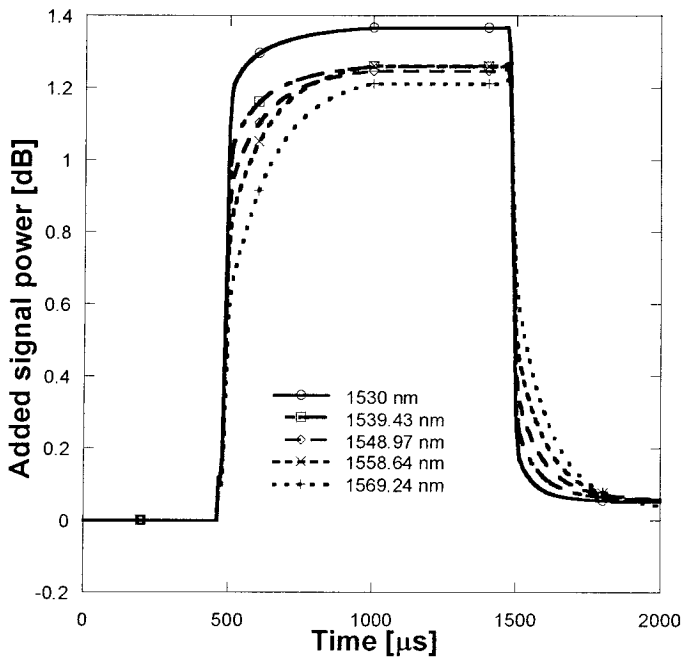

Figure 6.2 Surviving channel power fluctuation as a function of time when the L band out of L+C band channels are dropped/added.

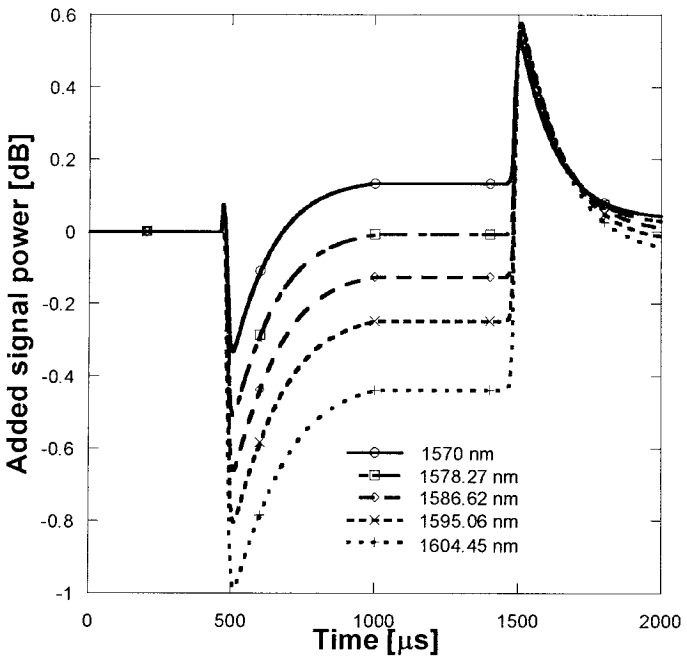

Figure 6.3 Surviving channel power fluctuation as a function of time when the C band out of L+C band channels are dropped/added.

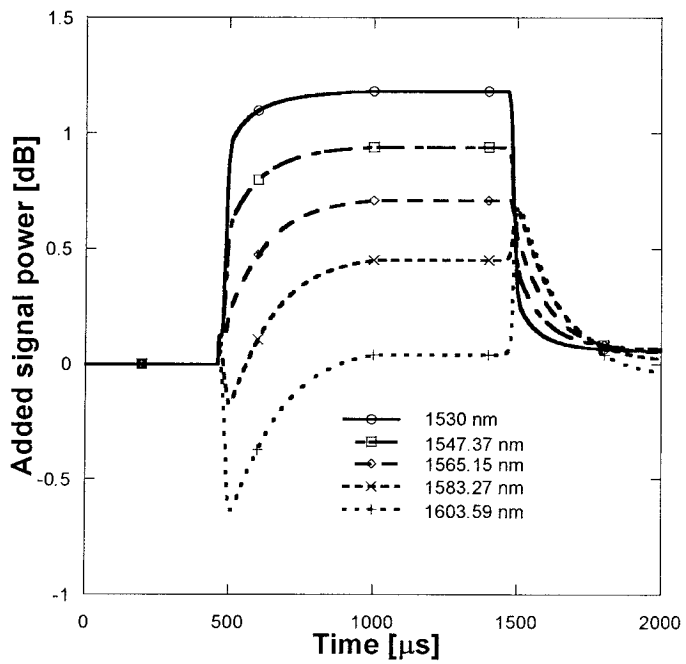

Figure 6.4 Surviving channel power fluctuation as a function of time when every second channel is dropped/added.

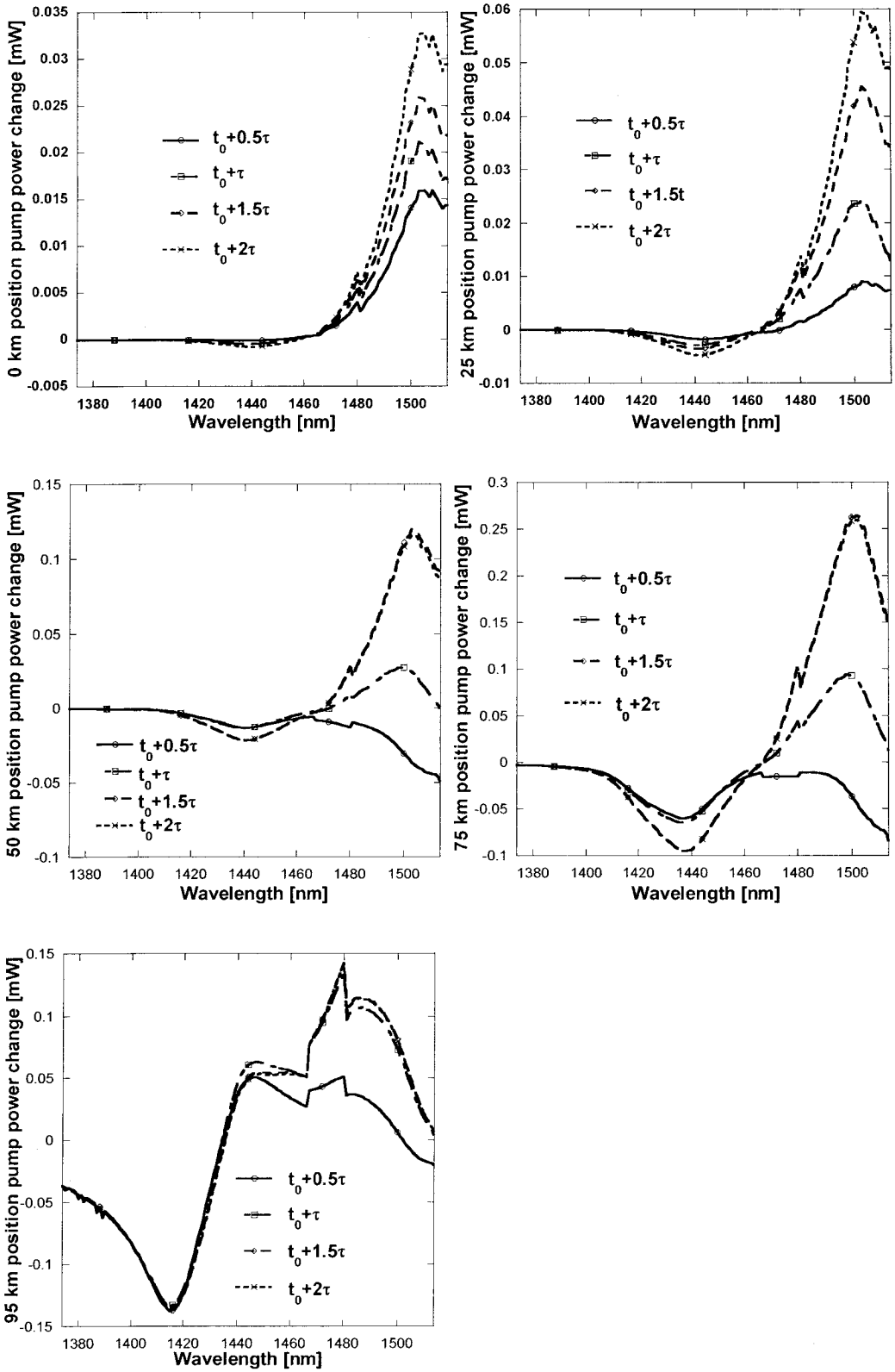

Figure 6.5 Distribution of pump power change at different position and at different instances of time when the L band out of L+C band channels are dropped/added.

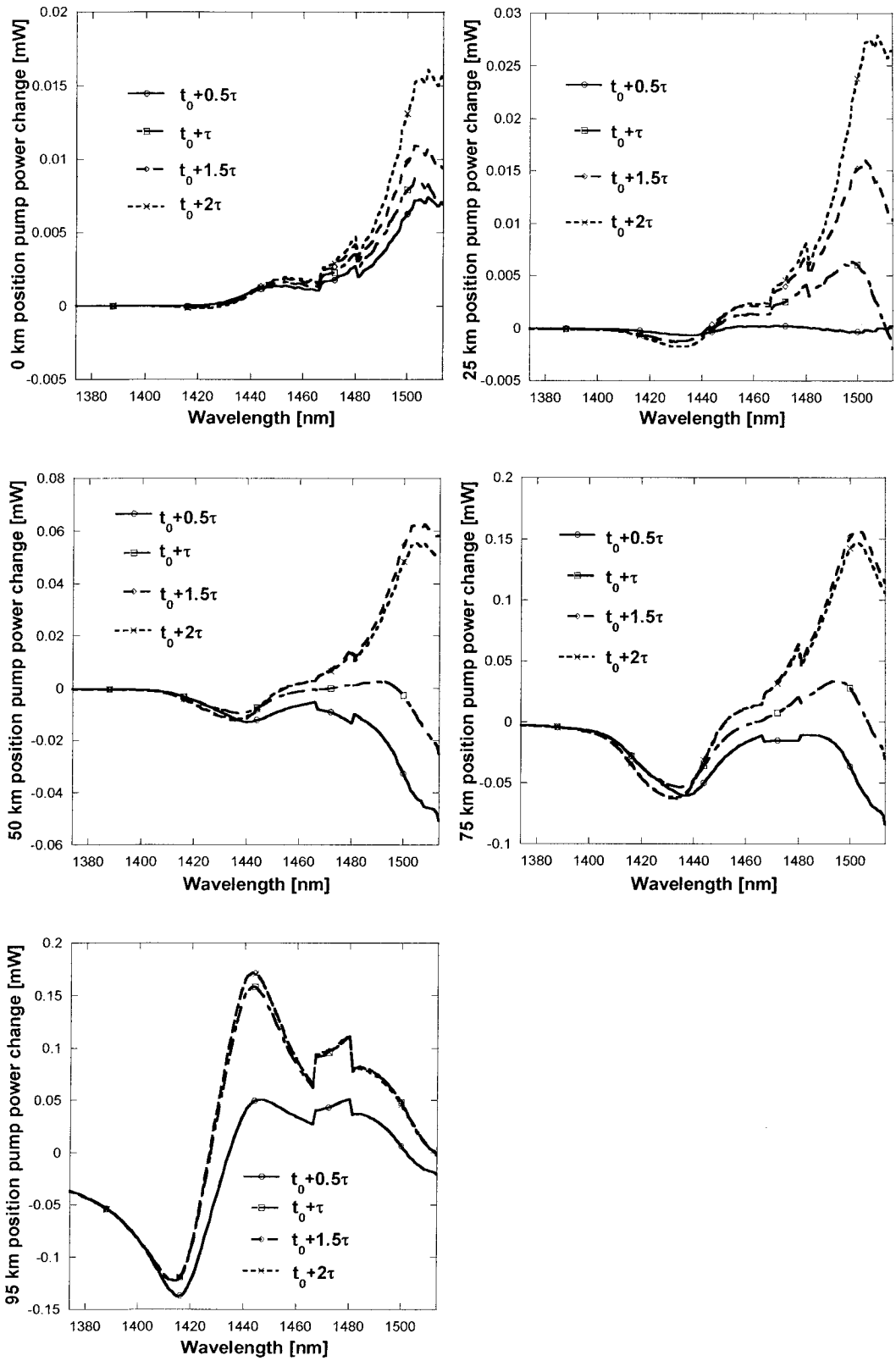

Figure 6.6 Distribution of pump power change at different position and at different instances of time when the C band out of L+C band channels are dropped/added.

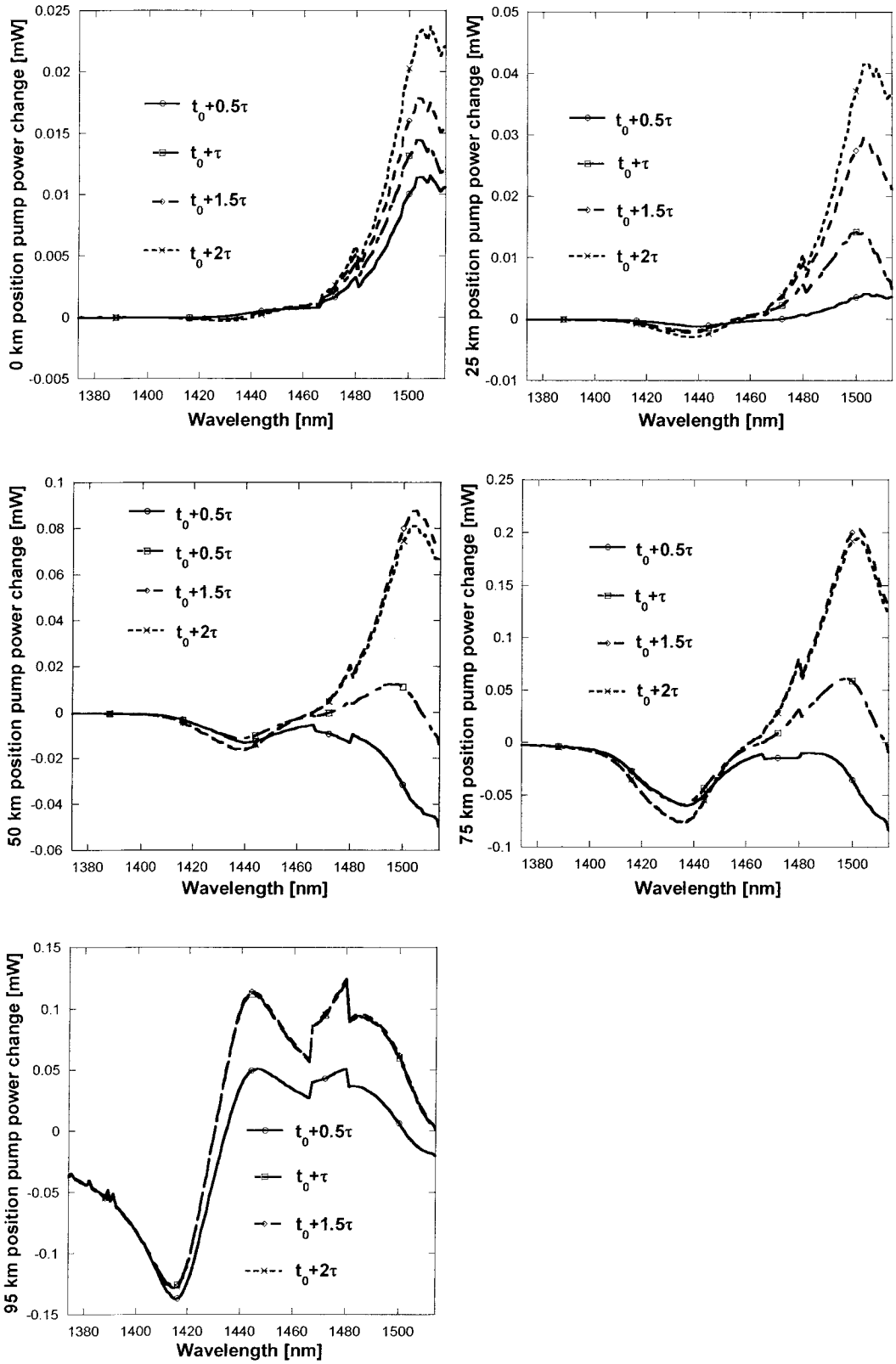

Figure 6.7 Distribution of pump power change at different position and at different instances of time when every other channel is dropped/added.

6.4 Comparison of power transients in fiber Raman amplifiers with multiple coherent pumping or incoherent pumping

We investigate the power transient characteristics of the FRAs with two incoherent pumps. The resulting on-off Raman gain is ~10 dB with a ripple of ~1 dB over 1530 – 1605 nm for FRAs with six coherent pumps or two incoherent pumps, shown in Figure 6.8 [39]. Corresponding to Figure 5.3, 5.4 and 5.5, Figure 6.2, 6.3 and 6.4 show the power transient behaviors of the FRAs with two incoherent pumps for the above three cases. For the case (a) as shown in Figure 6.2, it is seen that surviving signal power change or overshoot, particularly at the shorter wavelengths (e.g. 1530 nm) due to drop is more severe than that in Figure 5.3. This is because the pump power distribution of the two incoherent pumps is different from that of the six coherent pumps, and thus pump depletion change due to the drop of L-band signals is slightly different from that of the six coherent pumps. For the case (b) as shown in Figure 6.3, a slight undershoot at longer wavelength signals is observed due to the drop of C-band signals compared to the case (b) in Figure 5.4. But the overshoot due to the addition of C-band signals is almost the same as in Figure 5.4. For the case (c) as shown in Figure 6.4, there is no visible difference in power transient behaviors in FRAs with six coherent pumps or two incoherent pumps.

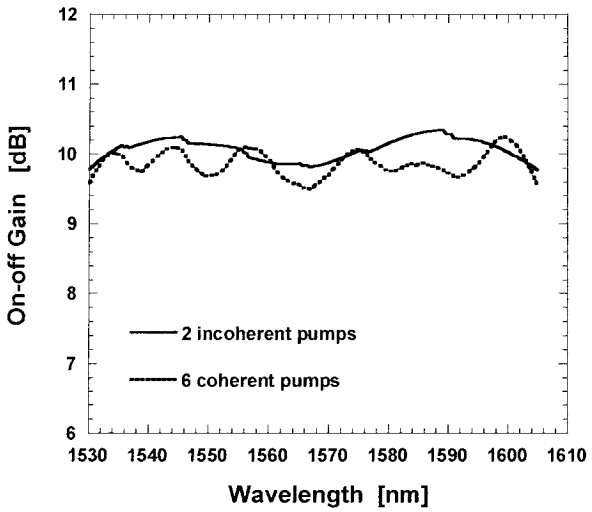

Figure 6.8 On-off Raman gain for the distributed FRAs with six coherent pumps or two incoherent pumps to cover the signal band of 1530 -1605 nm (C+L bands).

Chapter 7 Conclusion

Raman amplification is flexible in the sense that gain can be produced wherever there is optical fiber within a lightwave system. Furthermore, gain can be produced at any wavelength given the appropriate pump. This thesis presented a model for Raman amplifiers, which includes Raman emission and absorption processes. The model has been extended to support multiple pumps and signal wavelengths at both co-propagating and counter-propagating directions.

In this thesis, we investigate the effect of dropping/adding signal channels in FRAs on the dynamics of surviving channel power fluctuations. Our numerical model of fiber Raman amplifiers is based on the coupled non-linear partial differential equations that include pump-to-pump, pump-to-signal, and signal-to-signal Raman interactions, Rayleigh backscattering, wavelength dependent fiber loss, spontaneous emission noise and thermal noise. Surviving channel power excursion resulting from switching ON–OFF two out of four WDM channels has been studied, depending on pump configuration, the input power of signal channels, the length of the Raman fiber, the variable pump power. We analyze power transient as a function of fiber type. Because fiber type can affect pump depletion level, different fiber type has different transient behaviors. The power transients are analyzed in Raman amplifiers considering three pump configurations and addition/removal of different number of signal channels in a 6 channels-WDM system.

Three different cases are performed: (a) addition/removal of L band, (b) addition/removal of C band and (c) addition/removal of every other channel. For all three cases, power transient behaviors in distributed fiber Raman amplifier counter-pumped by multiple coherent pumps and multiple incoherent pumps have been analyzed at the same gain. Because pump power change due to addition or removal of signals determines the transient behaviors, and pump power distribution may be different between multiple coherent pumps and multiple incoherent pumps, it would be expected that power transient behaviors may be different in a FRA pumped by multiple coherent pumps or multiple incoherent pumps. It was shown that power transient behaviors of surviving signal channels are very similar for a FRA pumped by six coherent pumps or two incoherent pumps. However, a FRA with incoherent pumping suffers from slightly severer transients than that with multiple coherent pumps. We calculate the trend of coherent pump power change with different pump wavelengths, when some channel signals are dropped at an instant time. Our theoretical results demonstrate that the new steady-state pump power distribution is different from the previous steady-state pump power distribution with all channels on. The steady-state pump power distribution increases due to transient in longer wavelength pumps, while it decreases in shorter wavelength pumps. In case (a), (b), or (c), incoherent pump power changes are different. The new established area of shorter wavelength pump power compared with previous steady-state pump with the same pump wavelength power distribution area corresponding to all channels being on decreases due to energy transfer from shorter wavelength pump to longer wavelength pump. For the same reason, the new established area of longer wavelength pump power compared with previous steady-state pump with the same pump

wavelength power distribution area corresponding to all channels being on increases. In cases (a), (b), (c), the longer wavelength pump area power changes are different.

Our future work will focus on better control scheme to suppress the surviving signal channel transients according to pump power change along the fiber Raman amplifiers.

References

[1] G.P.Agrawal, Nonlinear Fiber Optics, 2nd ed. New York: Academic, 1995.

[2] S. G. Grubb, T. Strasser, W. Y. Cheung, W. A. Reed, V. Mizrachi, T.Erdogan, P. J. Lemaire, A. M. Vengsarkar, and D. J. DiGiovanni, "High power, 1.48 _m cascaded Raman laser in germanosilicate fibers," in *Proc. Optical Amplifiers and Their Applicat.*, 1995.

[3] N. W. Ashcroft and N. D. Mermin, *Solid State Physics*. Philadelphia, PA: Saunders College, 1976.

[4] R. H. Stolen, J. P. Gordon, W. J. Tomlinson, and H. A. Haus, "Raman response function of silica-core fibers," *J. Opt. Soc. Amer. B*, vol. 6, pp. 1159–1166, 1989.

[5] R. H. Stolen,"Polarization effects in fiber Raman and Brillouin lasers," *IEEE J. Quantum Electron.*, vol. QE-15, pp. 1157–1160, 1979.

[6] J. Yoshida, N. Tsukiji, A. Naki, T. Fukushima, and A. Kasukawa, "Highly reliable high power 1480 nm pump lasers," in *Testing, Reliability, and Application of Optoelectronic Devices*. Bellingham, WA: SPIE, Society of Photo-Optical Instrumentation Engineers, 2001, Proc. SPIE Volume 4285, pp. 146–158.

[7] A. Mathur, M. Ziari, and V. Dominic, "Record 1 watt fiber-coupled-power 1480 nm diode laser pump for Raman and erbium doped fiber amplification," in *Optical Fiber Communication Conf. OSA Tech.Dig.* Washington, DC, 2000.

[8] A. Yariv, *Quantum Electronics*, 3rd ed. New York: Wiley, 1989.

[9] S. A. E. Lewis, S. V. Chernikov, and J. R. Taylor, "Temperature-dependent gain and noise in fiber Raman amplifiers," *Opt. Lett.*, vol. 24, pp. 1823–1825, 1999.

[10] P. B. Hansen, L. Eskildsen, A. J. Stentz, T. A. Strasser, J. Judkins, J. J. DeMarco, R. Pedrazzani, and D. J. DiGiovanni, "Rayleigh scattering limitations in distributed Raman pre-amplifiers," *IEEE Photon. Technol. Lett.*, vol. 10, pp. 159–161, Jan. 1998.

[11] V. E. Perlin and H. G. Winful, "On distributed Raman amplification for ultrabroad-band long-haul WDM systems," *J. Lightwave Technol.*, vol. 20, pp. 409–416, 2002.

[12] Y. Emori, K. Tanaka, and S. Namiki, "100 nm bandwidth flat-gain Raman amplifiers pumped and gain-equalised by 12-wavelength-channel WDM laser diode unit," *Electron. Lett.*, vol. 35, pp. 1355–1356, 1999.

[13] H. Kidorf, K. Rottwitt, M. Nissov, M. Ma, and E. Rabarijaona, "Pump interactions in a 100-nm bandwidth Raman amplifier," *IEEE Photon.Technol. Lett.*, vol. 11, pp. 530–532, 1999.

[14] J. Bromage, P. J. Winzer, and R.-J. Essiambre, "Multiple path interference and its impact on system design," in *Raman Amplifiers for Telecommunications*, M. N. Islam, Ed. New York: Springer-Verlag, 2003, ch. 15.

[15] J. A. Armstrong, "Theory of interferometric analysis of laser phase noise," *J. Opt. Soc. Amer.*, vol. 56, pp. 1024–1031, 1966.

[16] J. L. Gimlett and N. K. Cheung, "Effects of phase-to-intensity noise conversion by multiple reflections on gigabit-per-second DFB laser transmission systems," *J. Lightwave Technol.*, vol. 7, pp. 888–895, 1989.

[17] C. H. Kim, J. Bromage, and R. M. Jopson, "Reflection-induced penalty in Raman amplified systems," *IEEE Photon. Technol. Lett.*, vol. 14, pp. 573–575, 2002.

[18] A. B. Puc, M. W. Chbat, J. D. Henrie, N. A. Weaver, H. Kim, A. Kaminski, A. Rahman, and H. A. Fevrier, "Long-haul WDM NRZ transmission at 10.7 Gb/s in S-band using cascade of lumped Raman amplifiers," in *Optical Fiber Communication Conf. OSA Tech. Dig.* Washington, DC, 2001.

[19] A. J. Stentz, T. Nielsen, S. G. Grubb, T. A. Strasser, and J. R. Pedrazzani, "Raman ring amplifier at 1.3 _m with analog-grade noise performance and an output power of 23 dBm," in *Proc. Optical Fiber Communications Conf.*, 1996.

[20] M. Ohashi, K. Shiraki, and K. Tajima, "Optical loss property of silicabased single-mode fibers," *J. Lightwave Technol.*, vol. 10, pp. 539–543, 1992.

[21] E. Brinkmeyer, "Analysis of the backscattering method for single-mode optical fibers," *J. Opt. Soc. Amer.*, vol. 70, pp. 1010–1012, 1980.

[22] A. H. Hartog and M. P. Gold, "On the theory of backscattering in single-mode optical fibers," *J. Lightwave Technol.*, vol. LT-2, pp.76–82, 1984.

[23] M. O. van Deventer, "Polarization properties of Rayleigh backscattering in single-mode fibers," *J. Lightwave Technol.*, vol. 11, pp. 1895–1899, 1993.

[24] C. R. S. Fludger and R. J. Mears, "Electrical measurements of multipath interference in distributed Raman amplifiers," *J. Lightwave Technol.*,ol. 19, pp. 536–545, 2001.

[25] D. Derickson, Ed., *Fiber Optic Test and Measurement*. Upper Saddle River, NJ: Prentice-Hall, 1998.

[26] P. J. Winzer, "Optical transmitters, receivers and noise," in *Wiley Encyclopediaof Telecommunications*, J. G. Proakis, Ed: Wiley, 2002, pp. 1824–1840.

[27] J. Bromage, C.-H. Kim, P. J. Winzer, L. E. Nelson, R.-J. Essiambre, and R. M. Jopson, "Relative impact of multiple-path interference and amplified spontaneous emission noise on optical receiver performance,"in *Proc. Optical Fiber Communication Conf.*, 2002.

[28] C. Martinelli, G. Charlet, L. Pierre, J. Antona, and D. Bayart, "System inpairment of double-Rayleigh scattering and dependence on modulation format," in *Proc. Optical Fiber Communications Conf.*, 2003.

[29] C. J. Rasmussen, F. Liu, R. J. S. Pedersen, and B. F. Jorgensen, "Theoretical and experimental studies of the influence of the number of crosstalk signals on the penalty caused by incoherent optical crosstalk," in *Proc.Optical Fiber Communications Conf.*, 1999.

[30] P. J. Winzer, R.-J. Essiambre, and J. Bromage, "Combined impact of double-Rayleigh backscatter and amplified spontaneous emission on receiver noise," in *Proc. Optical Fiber Communications Conf.*, 2002.

[31] R.-J. Essiambre, P. J. Winzer, J. Bromage, and C. H. Kim, "Design of bidirectionally pumped fiber amplifiers generating double Rayleigh backscattering," *IEEE Photon. Technol. Lett.*, vol. 14, pp. 914–916, 2002.

[32] A. K. Srivastava, J. L. Zyskind, Y. Sun, J. Ellson, G. Newsome, R. W. Tkach, A. R. Chraplyvy, J. W. Sulhoff, T. A. Strasser, C. Wolf, and J. R. Pedrazzani, "Fast-link control protection for surviving channels in multiwavelength otical networks," *IEEE Photon. Technol. Lett.*, vol. 9, pp. 1667–1669, Dec. 1997.

[33] C. J. Chen and W. S. Wong, "Transient effects in saturated Raman amplifiers," *Electron. Lett.*, vol. 37, no. 6, pp. 371–373, 2001.

[34] M. Karasek, J. Kanka, J. Radil, "Analysis of channel addition/removal response in all-optical gain-clamped cascade of lumped Raman fiber amplifier," J. Lightwave Technol., vol. 22, No. 10, pp.2271-2278, 2004

[35] Karásek, M., Kaňka, J., Honzátko, P., Radil, J.: Channel Addition/Removal Response in All-Optical Gain-Clamped Lumped Raman Fiber Amplifier. IEEE Photonics Technology Letters., vol.16, No. 3, pp.771-773, 2004

[36] Karásek, M., Kaňka, J., Honzáko, P., Radil, J.: Protection of Surviving Channels in All-Optical Gain-Clamped Lumped Raman Fibre Amplifier: Modelling and Experimentation. Optics Communications 231:No.1-2, pp.309-317, 2004

[37] M. Karásek, M. Menif, "Channel addition/removal response in Raman fiber amplifiers: modelling and experimentation" IEEE J. Lightwave Technol, vol. 20, No. 9, 1680-1687, 2002

[38] M. Karásek, M. Menif, "Protection of surviving channels in pump-controlled gain-locked Raman fibre amplifier", Optics Communications, vol. 210, 57-65, 1 September 2002.

[39] T. Zhang, X. Zhang, and G. Zhang, "Distributed fiber Raman amplifiers with incoherent pumping," *IEEE Photon. Tech. Lett.*, vol.17, no.6 pp. 2005.